MICHEL Guillaume

ECOLE NORMALE
SUPERIEURE DE PARIS

Training Course at LIGO 40m Lab in CALTECH

Stage de recherche, MIP 2^{eme} année

Development of Length Sensing and Control System for Advanced LIGO

Développement d'un système de controle en position des optiques pour Advanced-LIGO

January, 7^{th}-June, 29^{th} 2001

Supervisor:
A.J WEINSTEIN
California Institute of Technology
1200 E. California Blvd
PASADENA, CA 91125
ajw@hep.caltech.edu

July 22, 2001

Abstract

In this study, we have learned how to use the E2E simulation program and the Han2k model to design an “in lock” length sensing and control system for Initial-LIGO that can be generalized to Advanced-LIGO. Although this study is less general that previous for Initial-LIGO, it is a necessary step toward the generalization of that work for the Advanced-LIGO optical configuration.

This first length sensing and control system can be used to study the dynamic of laser field in Advanced-LIGO optical configuration using the E2E simulation program.

In this study, we have measured transfer functions of the interferometer, both open loop and closed loop. We have used this simulation program to better understand the control of a LIGO-like interferometer.

Résumé

Dans cette étude nous avons appris à utiliser le logiciel de simulation E2E et le modele Han2k pour développer un système de controle en position des optiques pour LIGO initial qui peut être généralisé à LIGO avancé. Bien que cette étude soit moins générale que la précédente pour LIGO initial, c'est un pas nécéssaire avant la généralisation de ce travail à la configuration optique de LIGO avancé.
Ce premier système de controle en position peut être utilisé dès à présent la dynamique du champ laser dans une configuration optique de type LIGO avancé.
Dans cette étude, nous avons mesuré des fonctions de transfert de l'interféromètre aussi bien en boucle ouverte que fermée et nous avons utilisé ce logiciel de simulation pour mieux conprendre comment controller un interféromètre de type LIGO.

Acknowledgments

- I would sincerely like to thank Alan WEINSTEIN for his welcome, his help during the period I was in the laboratory and also for his great help and corrections for this report.
- Thanks to Dennis UGOLINI for his precious time, for his friendship and for making me interested in American culture.
- Thanks a lot to Steve VASS for this wonderful days of work on the interferometer with laugh and friendship. I hope we can see each other again on the slopes.
- I would like to thank all the CALTECH LIGO engineers, I could meet during this six months for their welcome: Rick, Paul, Ben, Mike, Larry, Lee, Peter ...
- I would like to thank CALTECH and the LIGO project for the opportunity to enroll for six months as a visiting graduate student.
- Finally, I would like to thank Pierre-Francois CAHADON and Ricardo DESALVO for their help to find this job.

Contents

List of Figures

List of Tables

Chapter 1

Introduction

General theory of Relativity was published in 1916 by Albert Einstein. Since the sixties, many scientists have been trying to detect one phenomenon predicted by General Relativity that has never been confirmed: that is gravitational wave. Weber built a huge resonant bar to detect changes in its normal vibration modes due to a gravitational wave burst. Unfortunately, the gravitational waves are very hard to detect because the interaction with matter is very weak. None have been detected so far.

Since 1975, Taylor and Hulse have studied the pulsar PSR-1913+16 which has an unseen companion star. These two stars orbit around each other and the pulse of the pulsar (frequency 17Hz) is modulated at the frequency of the orbit (frequency around eight hours). The Theory of gravity from Newton says the modulation of the frequency of this pulse must be exactly constant if there is no friction (isolated system); Einstein's theory says the modulation of the frequency should rise because the system emits radiation (gravitational waves) which carry energy away causing the stars to spiral into each other. Taylor and Hulse measured the change of this frequency modulation over 25 years and compared these data to the prediction of the General Relativity: the agreement was excellent. They received the Nobel Price for the first indirect proof of the existence of gravitational waves.

Today, we want to measure directly the gravitational waves and use them to do astronomy. Gravitational waves are unique for astronomy because they interact poorly with matter and that can pass through dust and matter without alteration. Gravitational wave astronomy can see things that electromagnetic telescopes cannot see. In the early moment of the Big Bang, the universe was not transparent to electromagnetic radiation, so we cannot see the universe with electromagnetic radiation before the date when the universe became transparent to it. With gravitational wave we can see back to this early time (300 000 years after the Big Bang) and learn much more about the early moment of the Big Bang. Gravitational wave astronomy is a very useful tool to study extremely energetic events in the universe such as black holes because they emit a lot of gravitational waves that we can detect.

LIGO is one of a new type of gravitational wave detectors. Its purpose is to prove directly the existence of gravitational wave and to do astronomy with them. LIGO is a large Michelson interferometer (with 4 km arms) with suspended optics. Because of the quadrupolar property of the gravitational wave, it should change the length of the arms in opposite directions and then change the amount of light at the output (signal of a gravitational wave). Initial-LIGO will run from 2002 to 2006. It will then be upgraded to Advanced-LIGO with much greater sensitivity. The CALTECH 40m laboratory is developing a prototype of Advanced-LIGO optical configuration and control system. The purpose of this laboratory is to minimize the time to construct Advanced-LIGO.

I spent six months in the 40 meter laboratory at CALTECH (USA). My assignment was to develop the design of a length control system for Advanced-LIGO. Because it is hard task, we decided to limit the study to the "in lock" state as opposed to the development to the procedure for acquiring lock. We have started with Initial-LIGO and we have developed a control scheme for that interferometer. By the end, we have begun the study for Advanced-LIGO but more work has to be done.

Chapter 2

Background

2.1 What are gravitational waves ?

2.1.1 Gravitational wave equations

One of the predictions of the General theory of Relativity is the existence of a new type of wave: the gravitational wave. These waves are vibrations of space-time itself and propagate at the speed of light. Appendix B shows how to derive the gravitational wave equations from the Einstein's field equations. In the linearized theory of gravity, we can write the metric tensor $g_{\mu\nu}$ as:

$$g_{\mu\nu} = \eta_{\mu\nu} + h_{\mu\nu} \; with \; |h_{\mu\nu}| \ll 1, \tag{2.1}$$

where $\eta_{\mu\nu}$ is the metric tensor in flat space-time and $h_{\mu\nu}$ is a small perturbation.
After some algebra (see appendix B) we obtain, in Lorentz gauge:

$$\Box \bar{h}_{\mu\nu} = 0, \tag{2.2}$$

where $\bar{h}_{\mu\nu} = h_{\mu\nu} - \frac{1}{2} h \eta_{\mu\nu}$ is the reduced perturbation of the metric tensor and $\Box = \partial_\rho \partial^\rho$ is the d'Alembertian operator.
Equation 2.2 is a wave equation with plane wave solutions propagating at the speed of light. This equation is similar to electromagnetic wave equation except this one is a tensorial equation. This tensorial nature induces some new properties such as new type of polarizations.

2.1.2 Gravitational wave equations in the TT-gauge

Because the Lorentz gauge does not fix totally this equation, we can impose other gauge conditions. Usually, we use the Transverse-Traceless gauge because in this gauge, mathematics and physics are easier. By definition the Transverse-Traceless gauge (TT-gauge) is :

$$h_{\mu 0} = 0, \tag{2.3}$$
$$h_{kj,j} = 0, \tag{2.4}$$
$$h_{kk} = 0. \tag{2.5}$$

So $h_{\mu\nu} = \bar{h}_{\mu\nu} = h^{TT}_{\mu\nu}$ and after some calculation:

$$R_{j0k0} = -\frac{1}{2} h^{TT}_{jk,00}. \tag{2.6}$$

In this gauge with the Lorentz condition, only the spatial components h_{jk} are non-zero and h is divergenceless and traceless.
So a general plane wave solution propagating in z direction in the TT-gauge can be represented with two transverse polarizations by

$$h^{TT}_{\mu\nu} = \begin{pmatrix} 0 & 0 & 0 & 0 \\ 0 & h_+ & h_\times & 0 \\ 0 & h_\times & -h_+ & 0 \\ 0 & 0 & 0 & 0 \end{pmatrix} \tag{2.7}$$

where h_+ and $h_\times$ represent the amplitude of the $+$ and $\times$ polarization.

The Figures 2.1 and 2.2 show the effect of a gravitational wave arriving perpendicular to a material ring for the two different polarizations.

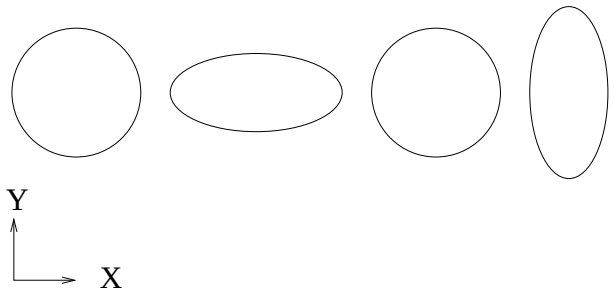

Figure 2.1: Effect of polarization + on material ring.

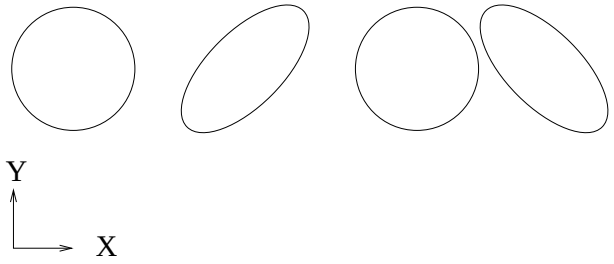

Figure 2.2: Effect of polarization $\times$ on material ring.

The effect on a Michelson interferometer with suspended mirrors is to stretch one arm and squeeze the other. LIGO exploits this property to detect gravitational waves. LIGO is a Michelson interferometer with free-falling test masses which are the two mirrors of the Michelson interferometer. We call these two mirrors ETM for End Test Mass . For a general gravitational wave incoming to one LIGO detector, the ETMs will move in a very specific way that we will describe later.

2.1.3 Behavior of gravitational wave under rotation

We consider without loss of generality the gravitational wave propagating along the z axis and we consider a rotation in the (xy) plane. After some algebra we have:

$$\begin{cases} h'_+ = cos(2\psi)h_+ + sin(2\psi)h_\times \\ h'_\times = -sin(2\psi)h_+ + cos(2\psi)h_\times \end{cases} \tag{2.8}$$

If we rotate the polarization angle ψ of π, h' remains unchanged. In quantum mechanics, this corresponds to a particle of spin 2 ($spin = \frac{2\pi}{angle\ of\ rotation}$). The elementary particle which is associated to the gravitational wave is the graviton. At present, there exists no experimental evidence for the graviton, neither for gravitational waves. This is because the coupling constant of the gravity is very small compared to the other force coupling constants. Since the gravitational wave travels at the speed of light, in the incomplete Quantum Theory of General Relativity, the graviton is expected to be massless.

2.1.4 Gravitational wave sources and LIGO science goals

The emission of gravitational waves is similar to that of electromagnetic waves in principle, though it is so much smaller in practice because of the weakness of the gravitational force compared to electromagnetism ($\sim 10^{-39}$ times weaker for

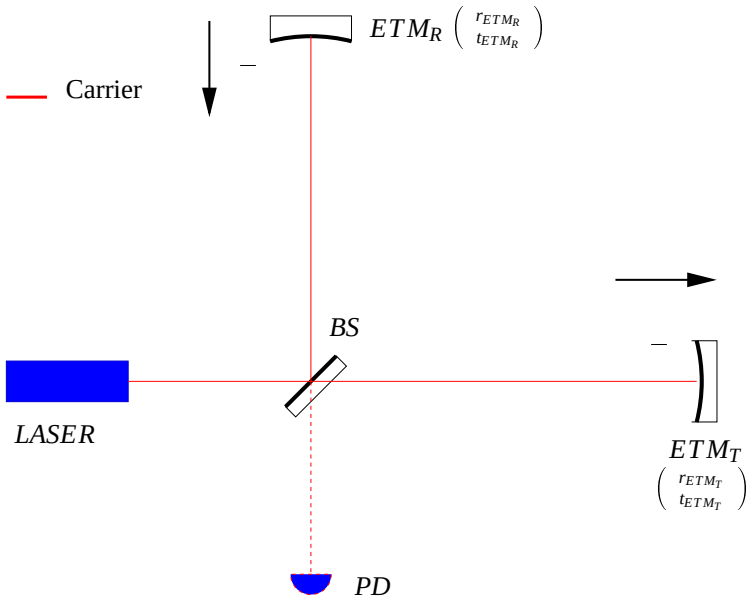

Figure 2.3: Effect of an orthogonal gravitational wave on a Michelson interferometer.

the force between a proton and an electron). Only very massive systems undergoing powerful accelerations, such as cataclysmic astrophysical events, will radiate detectable gravitational waves. There are three categories of gravitational radiation depending on the waveform: periodic sources (pulsars in orbit), bursts (supernovae, coalescences of neutron stars in spirals), stochastic sources (primordial gravitational waves from the Big Bang and incoherent superposition of many sources). The range of frequencies for periodic sources is, in theory, between 0 Hz and 10^{4} Hz but LIGO bandwidth is limited at low frequency by the seismic noise around $40Hz$ and at high frequency by the shot noise around $3000Hz$.
Gravitational waves are different from electromagnetic ones also because the gravitational dipolar moment is null because of conservation of linear and angular momenta. The energy in gravitational waves should therefore be dominated by quadruple radiation, which is proportional to the square of the third derivative of the ("reduced") quadruple moment as given in [5]:

$$\dddot{I} \sim \frac{(mass\ in\ motion)(system\ size)^2}{(system\ transit\ time)^3} \sim \frac{MR^2}{T^3} \sim \frac{(Non-spherical\ Energy)}{T} \tag{2.9}$$

Following [5], h is given by:

$$h \sim few\ x\ 10^{-21} \left(\frac{E_{non-spherical}}{M_{\odot}c^2}\right)\left(\frac{10\ Mpc}{r}\right) \tag{2.10}$$

This formula gives an approximation of the gravitational wave emission from a "typical" astrophysical source, as well as an estimation of the measurable gravitational wave induced strain cause by $\sim$ 1 $M_{\odot}$ of energy undergoing non-spherical motion at a distance from earth similar to the Virgo cluster of galaxies.

2.1.5 LIGO antenna pattern

LIGO is sensitive to gravitational waves from all directions in the sky and all polarizations. So we need to find the effect of the gravitational wave on our detector as a function of the position in the sky, polarization and type of the source.
To know the effect in the change of length in our interferometer, we use the geodesic deviation in a linearized gravitational wave (see [5] page 950-951).
In TT coordinate system that, to first order in the metric perturbation $h^{TT}{}_{jk}$, moves with the Beam Splitter and with its proper reference frame:

$$\frac{d^2\xi^j}{dt^2} = -R^{TT\,j}{}_{0k0}\xi^k\ with \begin{pmatrix} k & = & 1,2,3 \\ j & = & 1,2,3 \end{pmatrix}\ for\ x,y,z\ arms. \tag{2.11}$$

where ξ^j is the length of the j arm in the Beam Splitter (BS) proper frame. There is no z arm in LIGO so $\xi^3 = 0$ Eq. 2.6 and 2.11 give:

$$\frac{d^2\xi^j}{dt^2} = \frac{1}{2} h^{TT}{}_{j}{}_{k,00}\xi^k \tag{2.12}$$

Let (X,Y,Z) be the frame of reference attached to the gravitational wave and (x,y,z) the frame of reference attached to the detector. We will use the following convention :

- Capital latin letters for the gravitational wave,
- lower latin letters for the detector,

as in Schutz [12]. We use the main-convention for Euler angles:

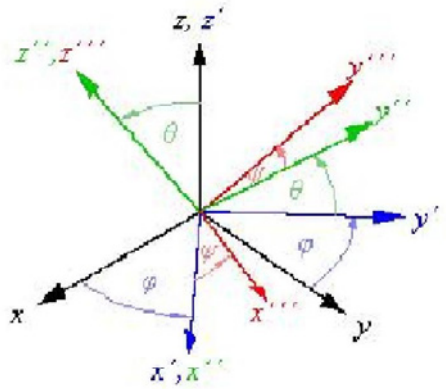

Figure 2.4: Main convention for Euler angles.

lets A^j_K the matrix of 3D-rotation to pass from (X,Y,Z) to (x,y,z).

$$A^k{}_K = \begin{pmatrix} cos(\phi)cos(\psi) - cos(\theta)sin(\phi)sin(\psi) & -cos(\psi)cos(\theta)sin(\phi) - cos(\phi)sin(\psi) & sin(\phi)sin(\theta) \\ sin(\phi)cos(\psi) + cos(\phi)cos(\theta)sin(\psi) & cos(\phi)cos(\psi)cos(\theta) - sin(\phi)sin(\psi) & cos(\phi)sin(\theta) \\ sin(\psi)sin(\theta) & cos(\psi)sin(\theta) & cos(\theta) \end{pmatrix}$$

so $\xi^i = A^i{}_R\xi^R$ and $\xi^K = ({}^TA)^K{}_j\xi^j$ are the ways to switch from one frame to the other. Then in (X,Y,Z) eq.2.12 is:

$$\frac{d^2\xi^K}{dt^2} = ({}^TA)^K{}_j\frac{d^2\xi^j}{dt^2} = \frac{1}{2} h^{TT}{}^K{}_{R,00}({}^TA)^R{}_i\xi^i. \tag{2.13}$$

After some algebra we obtain:

$$\frac{d^2\xi^K}{dt^2} = \frac{1}{2} A^k{}_K h^{TT}{}^K{}_{R,00}({}^TA)^R{}_i\xi^i. \tag{2.14}$$

This equation gives ξ if we know h and the position in the sky of the source. We assume $\xi^i(t) = \xi^i(0)$ in the right side since any correction of ξ^i depend on h_{ij} and will give higher order contributions. So we can integrate the differential equation to:

$$\boxed{\delta\xi^k = \xi^k(t) - \xi^k(0) = \tfrac{1}{2} A^k{}_K h^{TT}{}^K{}_R(t)({}^TA)^R{}_i\xi^i(0)}. \tag{2.15}$$

Eq 2.15 gives the variation of the length of the k-arm. After some algebra we have the effect on the detector:

$$\boxed{\frac{L_-}{L} = \tfrac{1}{2}\left(F^-_+(\phi,\theta,\psi)h_+ + F^-_\times(\phi,\theta,\psi)h_\times\right)}, \tag{2.16}$$

with :

$$\begin{cases} F^-_+(\phi,\theta,\psi) &= \frac{1}{2}cos(2\phi)cos(2\psi)(3+cos(2\theta)) - 2cos(\theta)sin(2\psi)sin(2\phi) \\ F^-_\times(\phi,\theta,\psi) &= -\frac{1}{2}cos(2\phi)sin(2\psi)(3+cos(2\theta)) - 2cos(\theta)cos(2\psi)sin(2\phi). \end{cases} \tag{2.17}$$

L_- is the difference the the variations of the length of the two arms. Eq 2.15 gives also L_+, sum of the lengths of the two arms:

$$\boxed{\frac{L_+}{L} = \frac{1}{2}\left(F_+^+(\phi,\theta,\psi)h_+ + F_\times^+(\phi,\theta,\psi)h_\times\right)}, \tag{2.18}$$

with:

$$\begin{cases} F_+^+(\phi,\theta,\psi) &= cos(2\psi)cos^2(\theta) \\ F_\times^-(\phi,\theta,\psi) &= -sin(2\psi)sin^2(\theta). \end{cases} \tag{2.19}$$

By monitoring these two degrees of freedom (L_- and L_+) and using at least four LIGO-like antenna, we can calculate the position in the sky of the source and have other informations about the source by extracting the waveform from the data. This will be one of the first methods used to determine the source position and gravitational waves polarizations.
Figures 2.5 and 2.6 show the angular sensitivity of the detector for the two degrees of freedom L_- and L_+.

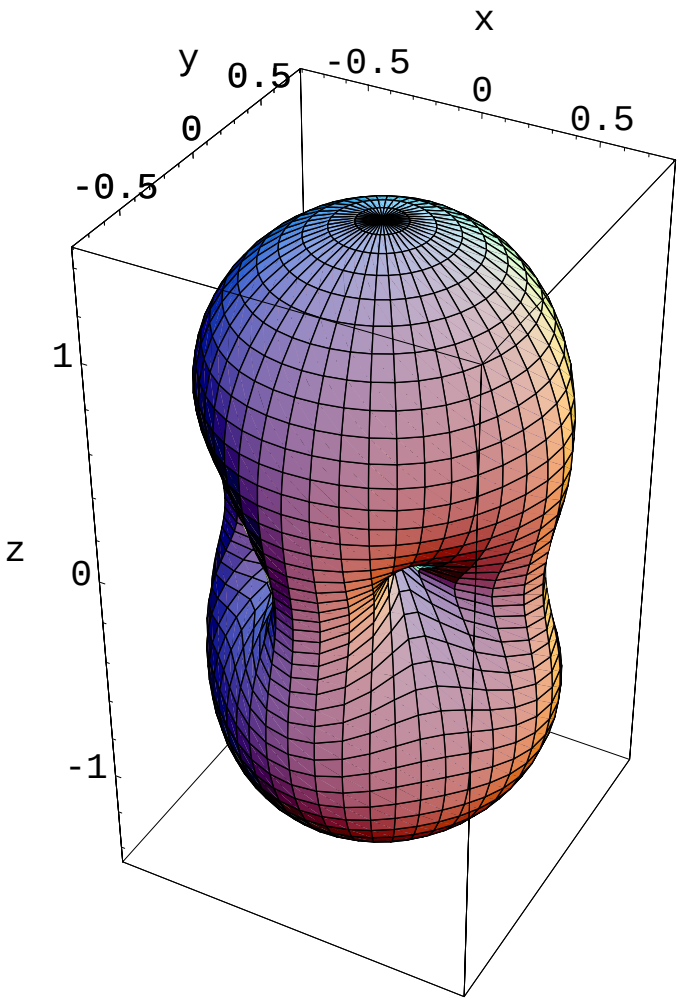

Figure 2.5: LIGO-like interferometer pattern for L_- with circular polarization.

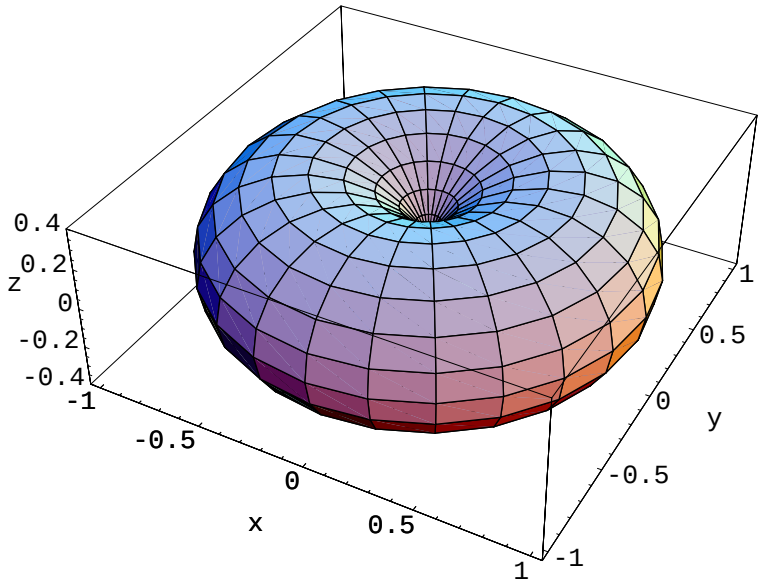

Figure 2.6: LIGO-like interferometer pattern for L_+ with circular polarization.

These figures show that gravitational interferometer are not very directional and that L_- and L_+ complete each other. Note, that LIGO is much less sensitive in L_+ than in L_-, since the laser frequency noise contributes mainly to the former.

2.2 Factors affecting interferometer sensitivity

The sensitivity of a gravitational wave interferometer is given by the ratio of signal to noise. So there are two ways to increase the sensitivity:

- increasing the signal output.
- decreasing the noise in the interferometer.

To increase the signal, we can:

- build an interferometer with long arms: for LIGO it is 4 kilometers long but the length cannot be increased indefinitely without severely limiting the bandwidth as discussed later,
- increase the laser power,
- noise must be reduced as much as possible. All technical sources of noise must be kept below the fundamental noise sources as described briefly below.

2.2.1 optical noise

One of the problems in detecting gravitational waves with interferometers is we can't differentiate a gravitational wave signal from phase fluctuation in our laser except for a perfect Michelson interferometer. To avoid the problem we use a laser as stable as possible, but there is two optical fundamental limits which affect directly the process of measurement.

shot noise

Shot noise is the dominant noise at high frequency, typically above a few hundred Hertz for LIGO. This is due to the random nature of light as described by quantum mechanics. Finite photons' statistics appears as a phase fluctuation in the Michelson interferometer.

The quantum fluctuation in the photons' statistics is proportional to $\sqrt{N}$ where $\bar{N}$ is the average number of photons exiting the asymmetric port of the Michelson interferometer due to the passage of a gravitational wave. So the fractional photon number fluctuation is proportional to $\frac{1}{\sqrt{P_{in}}}$ where P_in is the laser input power. Then, to increase our interferometer sensitivity we use a laser with the highest power we can build keeping in mind we also want a stable laser and we want to limit the thermal loading into our optics. The new laser of the 40m prototype is an infrared laser (Nd:YAG) with $\lambda = 1.064 \mu m$. The nominal output power is in order of 11 W in a circular TEM_{00} mode and the total output power in all modes except the circular TEM_{00} mode should be less than 500 mW. The amplitude spectral density of the fractional light power fluctuations at the input of the Input/Output Optics (IOO) should be $\frac{\delta P(f)}{P} < 10^{-6}\ Hz^{-\frac{1}{2}}$ for $100\ Hz < f < 10\ kHz$ and rising as $f^{-\frac{3}{2}}$ for $40\ Hz < f < 100\ Hz$ but at this point no test have been made because we are still installing the laser.

Radiation Pressure noise

If shot noise was the only limit to precision determined by the optical power P_{in}, then we could in principle achieve arbitrary precision simply by using a sufficiently powerful laser. But in addition to the substantial technical problems of high power lasers, there is an other fundamental limits on the precision of a measurement: radiation pressure noise. This limit is a consequence of the quantum consideration: how the measurement process disturbs the system under measurement? The laser light pushes the mirrors with a force $F_{rad} = \frac{P}{c}$ and the fluctuation due to shot noise in P gives an amplitude spectral density proportional to $\frac{\sqrt{P_{in}}}{f^2}$. So by increasing P_{in} we also increase the radiation pressure noise. There is an optimal power which leads to a minimum optical noise: $P_{opt} = \pi mc\lambda f^2$. For $m = 10\ kg$, $f = 100\ Hz$ and $\lambda = 1.064\ \mu m$, $P_{opt} = 1MW$ which is far higher than Initial-LIGO will operate with. So this class of detector will operate well below their optimal power and they will have shot noise bigger than the fundamental limit but LIGO II will be quantum limited.

2.2.2 Seismic noise

To detect gravitational waves, we use free-falling masses and monitor their displacement with a Michelson interferometer. Seismic motion produces noise in the motion of the mirrors. To eliminate as much as possible this noise we use at the sites passive seismic isolation stacks and pendulum suspension in order to reduce the noise at low frequency. Typically, an attenuation of $\frac{1}{f^8}$ is achieved above $50Hz$. At the 40m interferometer with use also active seismic isolation which achieves a 30dB attenuation at low frequency to 100 Hz. We use it because in California the human activity is much bigger than at the sites . Actually, seismic noise is our main noise at low frequency and prevents measurements under 40 Hz for LIGO I and $50Hz$ for the 40m interferometer.

2.2.3 Thermal noise

Another fundamental noise is due to the fact that the optics are at finite temperature which cause the wires which suspend the mirrors and the mirrors themselves to vibrate, introducing noise . The wire vibration is referred as "suspension thermal noise" and the mirror's vibration as "internal thermal noise". A way to decrease this noise is to use the least number of wires as possible, in this case it is one loop of wire per mirror and attach them as stiffly as possible to the mirror in order to minimize dissipation of thermal energy. We use also high Q mirrors so that the thermal energy is constrained to stay in the normal modes of oscillation of the mirrors masses, at frequencies above the LIGO sensitivity band. For LIGO I we use high uniformity fused silica quartz mirrors (Q up to 10^6) but for LIGO II we may use sapphire mirror which have better Q (Q up to 10^8).

2.3 Gravitational wave interferometer: LIGO

Many detectors are being built now all around the world. The main projects are LIGO (three antenna in the USA), VIRGO (one antenna in Italy), GEO600 in Germany and TAMA in Japan and ACIGA in Australia. To achieve the desired sensitivity, many techniques are used to get as close as possible to the fundamental and technical limits. This chapter gives an overview of the development of gravitational wave detectors. The purpose of this chapter is to show how to increase the sensitivity of the detector and how the fundamental limits can be reached by developing more elaborate methods.
Two parameters govern the optical response of the interferometer:

- the storage time limit
- the energy storage limit

2.3.1 Frequency response and time limit

To maximize the phase shift of light due to interaction with a gravitational wave, the interaction time must be optimized. The optimum interaction time is equal to $\frac{\tau_g}{2}$ where τ_g is the period of the gravitational wave. If the storage time of the light in the interferometer is longer than the gravitational wave's period, the length perturbation changes sign and begins to undo the phase shift imparted in the first half of the period. For a gravitational wave of frequency 500 Hz, the ideal time storage is equal to 1 ms. In 1 ms light travels 300 km, so the ideal arm length for a detector optimized for gravitational waves at 500 Hz is 150 km which is much longer than is feasible for a ground based interferometer.
One method to increase the effective length of the arm is to fold the interferometer arms. Two solutions have been found:

- using delay lines
- using Fabry-Perot cavities.

using these methods, the light travels N bounces in the arms before being recombined at the beam splitter. The effective length becomes $(N+1)L$ where L is the real length of the arms. The storage time is increased by a factor of $\frac{N+1}{2}$ compared to the single bounce case. Using delay lines in long interferometers is difficult because for N bounces we need N spots on the end test mirror. The size of one spot corresponding to diffraction limit, and the actual size of practical mirrors, make it impossible to have large N. Any overlap of the spot will induce interferences in the delay-lines which would modify the phase shift induced by the gravitational wave. The way LIGO achieves the required storage time is to use Fabry-Perot cavities in the arms of the interferometer.

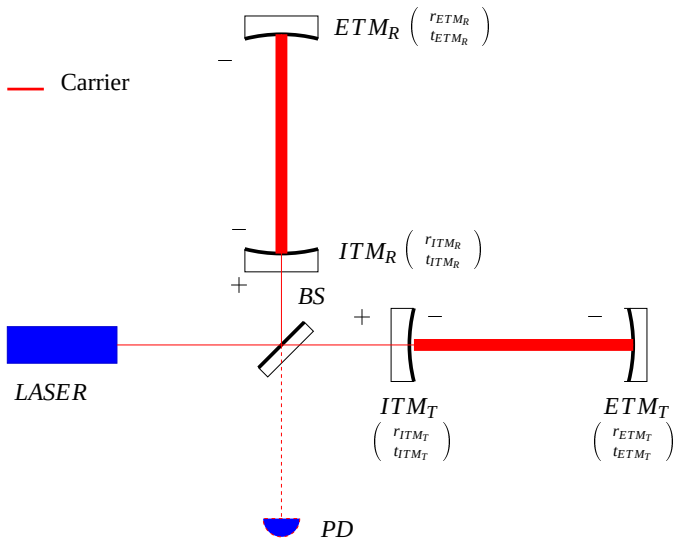

Figure 2.7: Fabry-Perot arm interferometer.

This solution allows smaller mirrors and the storage time of the arm cavity can be matched to the optimum storage time by adjusting the reflectivity of the input mirror. Thus arm cavities improve the sensitivity of the detector by reaching the optimum storage time but induce some difficulties like alignment and control. An arms cavity interferometer now has three degrees of freedom: two arms cavities length which must be held on resonance and the dark fringe condition of the Michelson interferometer. There are thus three length we have to control:

- $L_- = \Delta L_T - \Delta L_R$,
- $L_+ = \Delta L_T + \Delta L_R$,

- $l_- = position\ of\ ITM_T - position\ of\ ITM_R$

where $\Delta L_T = position\ of\ ETM_T - position\ of\ ITM_T$, $\Delta L_R = position\ of\ ETM_R - position\ of\ ITM_R$, ETM stands for End Test Mass, ITM stands for Input Test Mass, subscript R for the arm using light reflected through the beam splitter and subscript T for the arm using light transmitted through the beam splitter. The expense in using arm cavities is now the bandwidth of our detector is governed by the arm cavities. The arm cavities works as low pass filters so they increase the sensitivity at low frequency but decrease the sensitivity at high frequency.

2.3.2 Energy storage

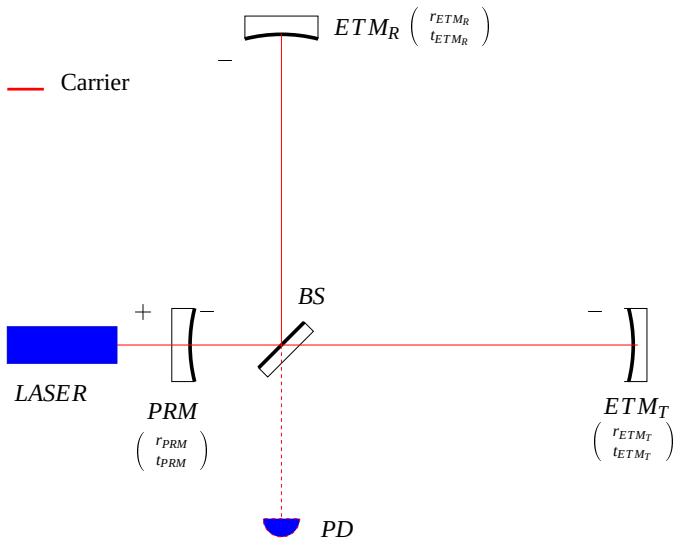

Figure 2.8: Power recycling interferometer.

As we saw in section 2.2.1, to minimize the influence of shot noise we need to use the most powerful laser possible. So we want the highest amount of energy stored in the interferometer as possible. The technique of power recycling has been invented for this purpose. This method consists in adding another mirror between the laser and the beam splitter. In the absence of gravitational waves, the interferometer is set to be at the dark fringe, so all the light is sent back to the laser. This new mirror sends back the light in phase with the new light from the laser to be re-used. This method increases the energy stored in the interferometer.
As a result there is an other degree of freedom to control (the position of the recycling mirror) and this mirror couples the two arms. A Michelson interferometer with power recycling can be see as a Fabry-Perot cavity composed of the power recycling mirror and another mirror equivalent to the rest of the interferometer.
Another problem is we increase also the temperature of the mirrors and so increase the thermal lensing effect. Any way, this method is still an improvement and does not change the bandwidth of our detector . By setting the reflectivity of this mirror in order to equal the total losses in the interferometer and the transmission of this mirror, we can maximize the circulating power in the interferometer. With this technique we can increase by a factor of fifty the power at the beam splitter.

2.3.3 Initial-LIGO optical Configuration

By combining the arm cavity and power recycling configurations, we can optimize both the storage time and the energy storage. This is the configuration for LIGO, VIRGO and TAMA. Four degrees of freedom must be controlled:

- differential mode in the arms (L_-),
- common mode in the arms (L_+),

- differential mode for the Michelson(l_-),
- common mode for the Michelson(l_+).

LIGO uses a single modulation frequency to obtain the four degrees of freedom by demodulation of the photocurrents at the reflected port, the pick-off in the power recycling cavity and the anti-symmetric port. LIGO operate for the detection of gravitational waves when the arms are resonant for the carrier but not for the sidebands, the power recycling cavity is resonant for the carrier and the sidebands and the anti-symmetric port is dark for the carrier (Schnupp asymmetry). Figure 2.9 shows the fields and the optical configuration of LIGO I.

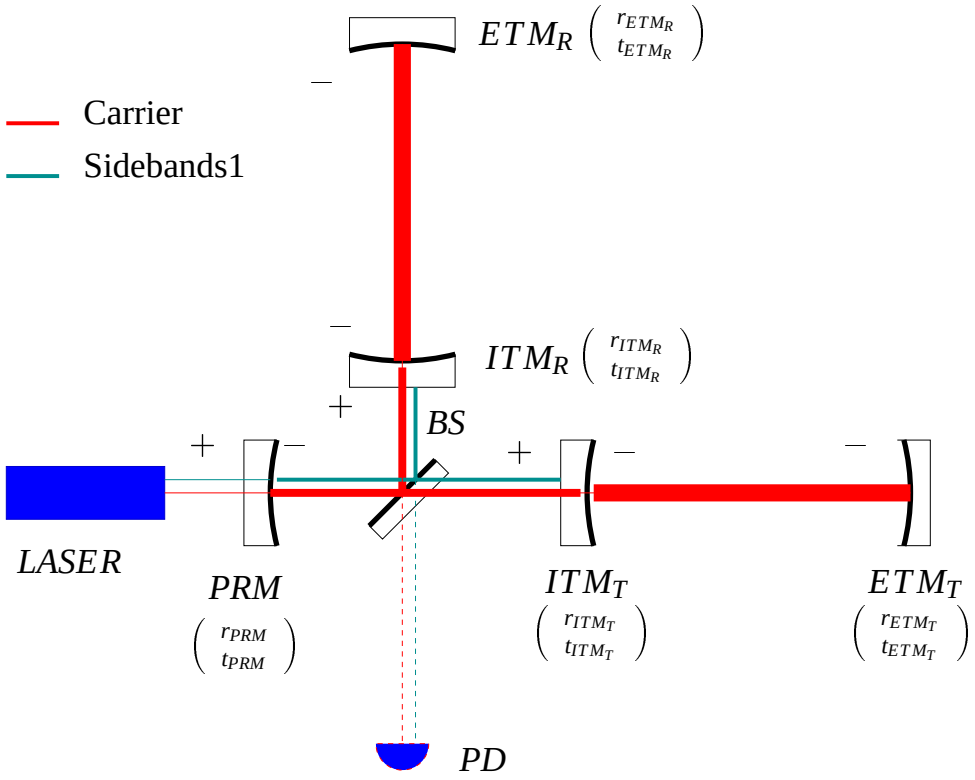

Figure 2.9: LIGO I optics configuration.

Quantity	Value(s)
Laser wavelength	$1.064\ \mu m$ (Nd:YAG)
Beam waist Diameter	$7.02cm$
Cavities Lengths	$L_{arm} = 2009m$ $Length\ from\ PRC\ to\ BS = 3.022m$ $Length\ form\ BS\ to\ ITMT = 9.82849m$ $Length\ form\ BS\ to\ ITMR = 9.52849m$ $Schnupp\ assym = 0.3m$
Mirror intensity transmissions	$T_{PRC} = 0.028$ $T_{ITM} = 0.028$ $T_{ETM} = 5.10^{-6}$ $T_{BS} = 0.49985$
Mirror intensity losses (design)	$L_{PRC} = 10^{-3}$ $L_{ITM} = 7.10^{-5}$ $L_{ETM} = 7.10^{-5}$ $L_{BS} = 3.10^{-4}$

Table 2.1: Typical parameter values for Initial-LIGO at Hanford 2Km.

2.3.4 Signal recycling and Resonant Sideband Extraction (RSE)

The signal sidebands induced by a gravitational wave do not see the power recycling mirror because they exit thru the anti-symmetric port. So the power recycling mirror does not affect the time storage of our signal. We can put a new mirror at the anti-symmetric port to optimize the storage time of the signal sidebands. With this configuration, we can optimize "independently" the storage time for the carrier and the storage time of the signal sidebands. Signal recycling can be used to tune the frequency response of our detector. We can make the frequency response large and have less sensitivity by decreasing the time storage of the signal sidebands (broad-band mode RSE) or choose a frequency and make the frequency response much more sensitive but narrower (signal recycling).
Figure 2.10 and 2.11 show the effect of tuning the signal recycling cavity by doing a microscopic shift of the signal recycling mirror:

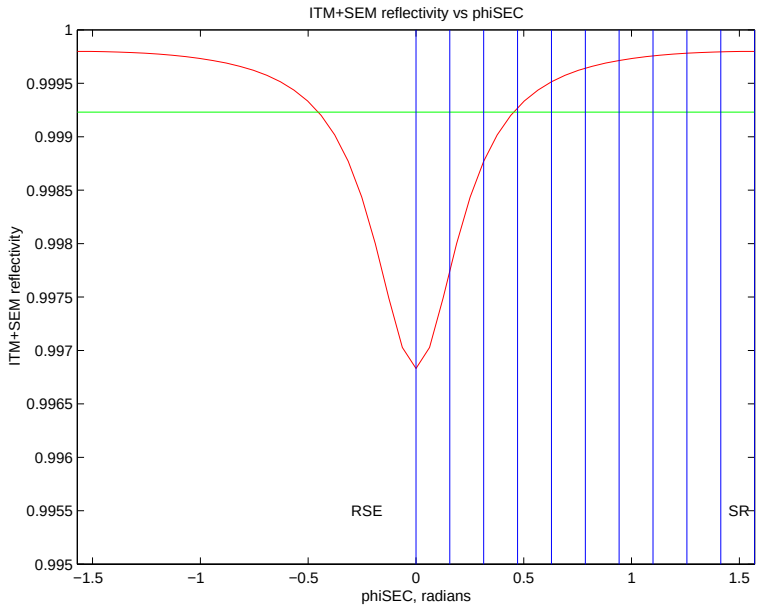

Figure 2.10: Amplitude reflectivity of the compound mirror formed by the ITM plus SM for different detunings.

The green horizontal line is the ITM reflectivity. The vertical lines indicate detunings ϕ_{SRC} in radians which correspond to the shot noise curves in the next figure.

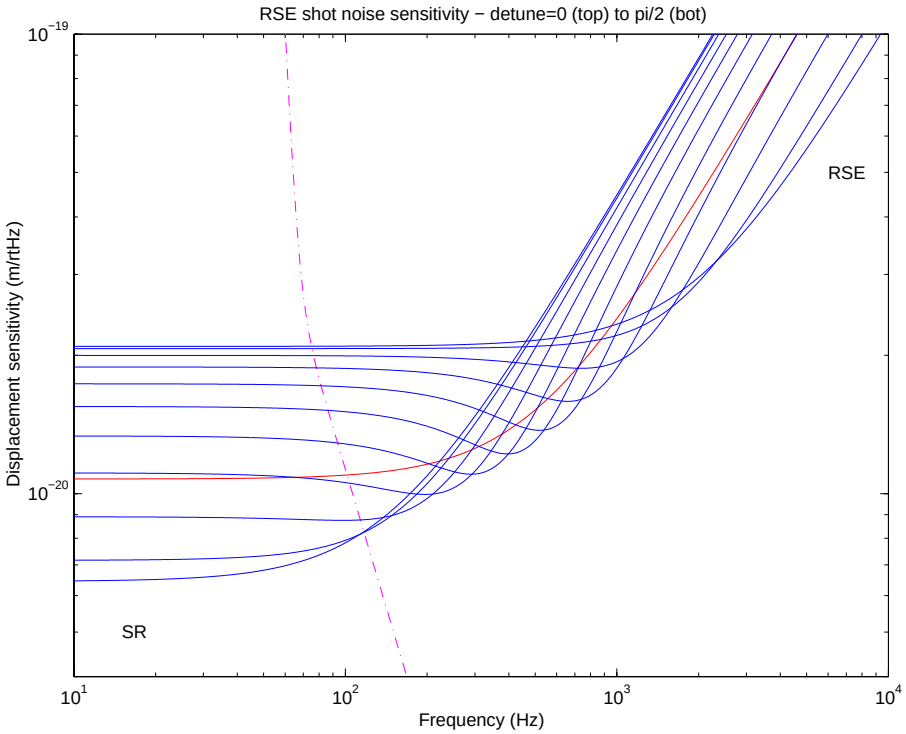

Figure 2.11: Shot noise displacement sensitivity versus GW frequency, for different SRC detunings.

The middle, red curve, with no dip, corresponds to the absence of SM; the other blue curves are in the presence of a SM, with tunes corresponding to the vertical lines in figure 2.10. They range from the narrow-band, $\phi_{SRC} = \pi/2$, "signal recycling" SR limit(bottom-most curve on the left), to the widest-band, $\phi_{SRC} = 0$ "resonant sideband extraction" RSE limit. The dash line represents the other noise displacement sensitivity.
A problem is that this extra mirror adds a new degree of freedom we have to control, and this mirror couples all the fields in the interferometer.
The set of power recycling and signal recycling is known as dual recycling.

2.3.5 Advanced-LIGO optical configuration

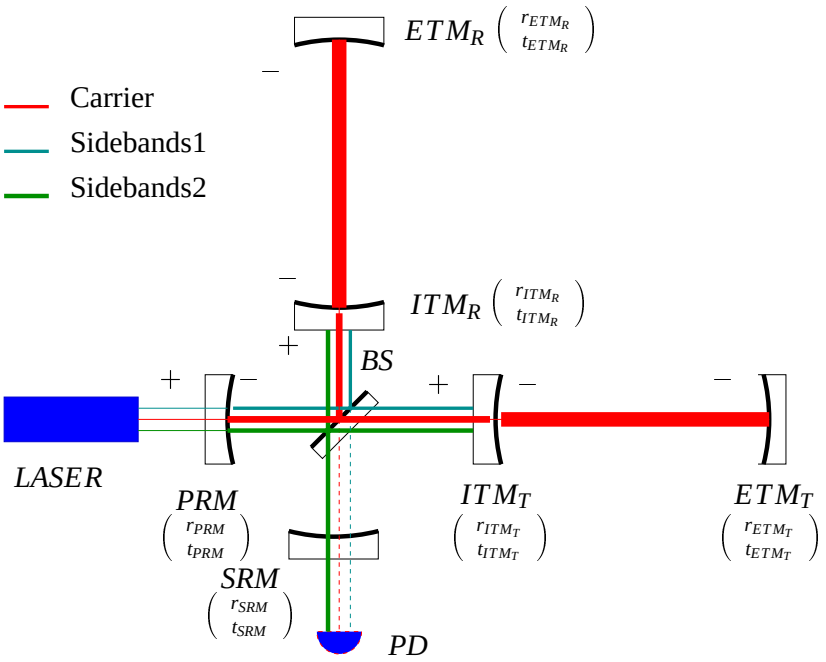

Figure 2.12: advanced-LIGO optical configuration.

Advanced-LIGO is the next generation of detector. Basically, it is an improved Initial-LIGO with a signal recycling mirror. Advanced-LIGO will be operational in 2006, and will improve by an order of magnitude the sensitivity of Initial-LIGO. The major improvements are:

- Better core optics (sapphire)
- Better suspensions and active seismic isolation
- Thermal lensing correction
- More powerful laser
- Dual recycling

The 40m Lab in CALTECH is a prototype of Advanced-LIGO in order to test the control scheme and suspended signal recycling configuration. In order to control 5 degrees of freedom (L^-, L^+, l^-, l^+ and l_s), we use two pairs of sidebands. The carrier is resonant in the arms and in the power recycling cavity and the anti-symmetric port is dark for the carrier. The first pair of sidebands is resonant in the power recycling cavity but not in the arms and the anti-symmetric port is dark for the first pair of sidebands. The second pair of sidebands is resonant in the power recycling cavity and the signal recycling cavity but not in the arms and the anti-symmetric is bright for this pair of sidebands. In beating the two sidebands with the carrier, we can extract the control signals for all the mirrors.

Quantity	Value(s)
Laser wavelength	$1.064\ \mu m$ (Nd:YAG)
Laser power	$125W$
Cavities Lengths	$L_{arm} = 4000m$ $Length\ from\ PRC\ to\ BS = 8.3276m$ $Length\ form\ BS\ to\ ITM_T = 4.4918m$ $Length\ form\ BS\ to\ ITM_R = 4.9082m$ $Length\ form\ BS\ to\ SRM = 9.1444m$ $Schnupp\ assym = 0.4164m$ $detuning = 0.0382$
Mirror's intensity transmissions	$T_{PRM} = 0.075$ $T_{ITM} = 0.005$ $T_{ETM} = 15.10^{-6}$ $T_{BS} = 0.49985$

Table 2.2: Typical parameter values for Advanced-LIGO at Hanford 4Km.

Chapter 3

Development of length sensing and control system for Advanced LIGO

Advanced LIGO will be the next generation of Michelson interferometer in the LIGO project. The purpose of the 40m Michelson interferometer is to prototype the control scheme for Advanced LIGO and to test the suspended dual recycling configuration with this control scheme and to debug the problems Advanced LIGO may encounter. At the time when I write this paper, we don't have any main core optics and also don't have a mode cleaner. We are installing and commission our pre-stabilized LASER (PSL) and our vacuum system. As far as I know, There is no control system for dual recycling configuration and the purpose of this research is to start to design one. Because it is a long and difficult job, we have started from Initial-LIGO configuration and try to design a control system to stay "in lock" which means all the fields are resonant in the cavities we want them to be resonant in, in other words all the mirrors are at the right place. I had some problem to design such a control system and I will expose the issues later. Because of these problems I did not have time to move to the Advanced-LIGO configuration but this job is a starting point to study dual recycling configuration.

3.1 End-to-End (E2E) simulation program and the Han2k model:

E2E is a very powerful simulation program based on C++. It has been developed by Hiro Yamamoto, Biplab Bhawal, Matt Evans, Edward Maros and Malik Rahkmanov ([1],[2],[3],[4]) in order to simulate interferometers such as Initial LIGO and Advanced LIGO. E2E can take in account LASER fields propagation, suspension effects, mirrors, photo-detectors and many other things around LIGO-like detectors.
From the user's point of view, E2E is mainly divided into two parts:

- A graphical interface called ALFI4 to setup the model,
- A program called modeler to run the model in the time domain.

The first thing to do is to design a model for the system we study. Most of my work during these past six months, have been done with the Han2k model which is supposed to represent the Hanford interferometer with 2*km* arms. Han2k model is purely a one dimension model: longitudinal (length) degrees of freedom. My job was to design a control system to stay "in lock" for Han2k. Even though it has already been done in a much more general study by Matt EVANS [8], this is the first step to understand how to build a control system for Advanced-LIGO. Figures 3.1, 3.2, 3.3, 3.4, 3.5, 3.6 and 3.7 show how the ALFI graphical user interface represents the model of the interferometer.

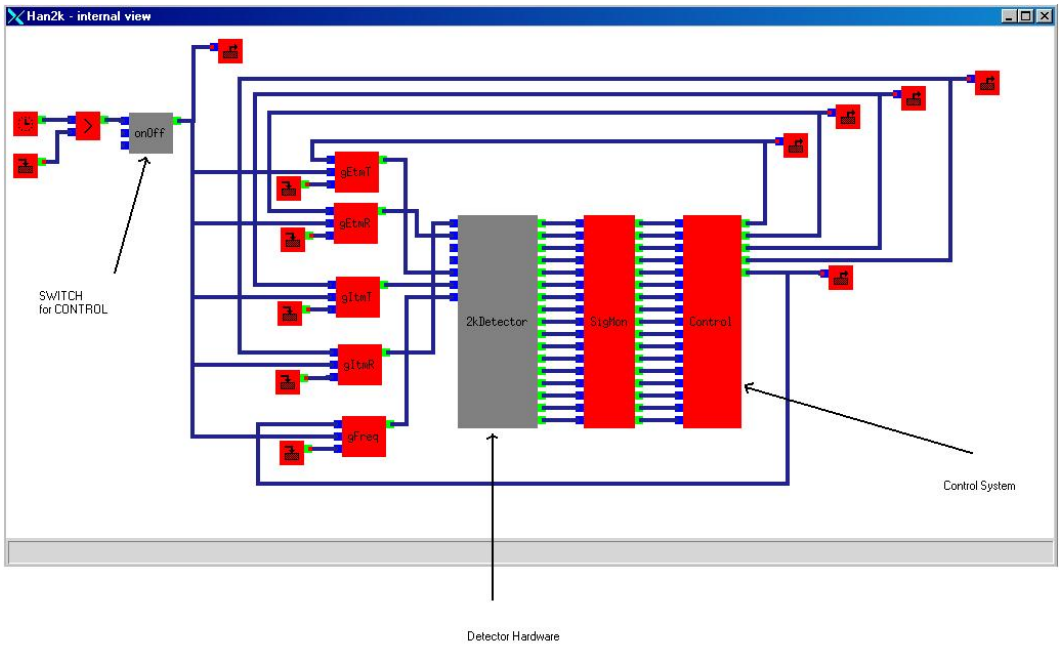

Figure 3.1: Main box for Han2k model.

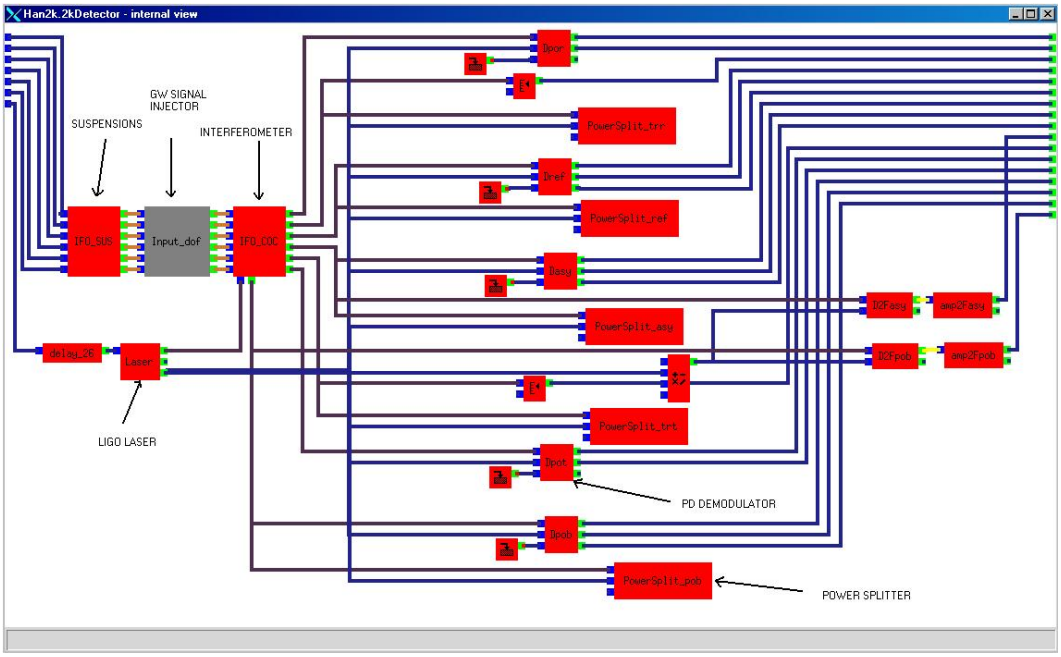

Figure 3.2: 2kDetector box.

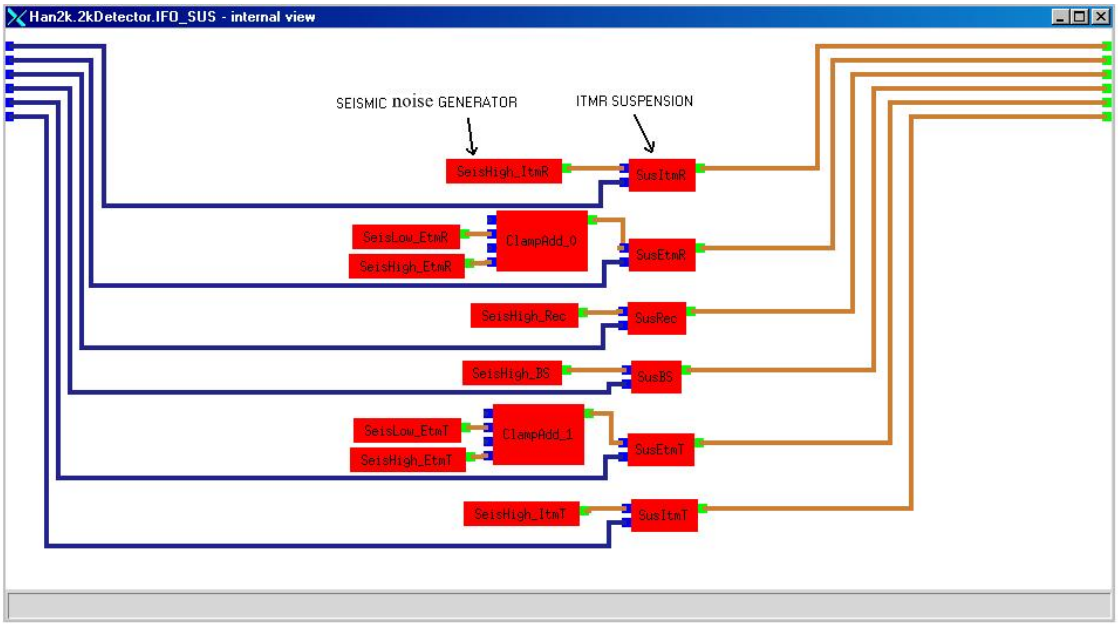

Figure 3.3: Suspensions box.

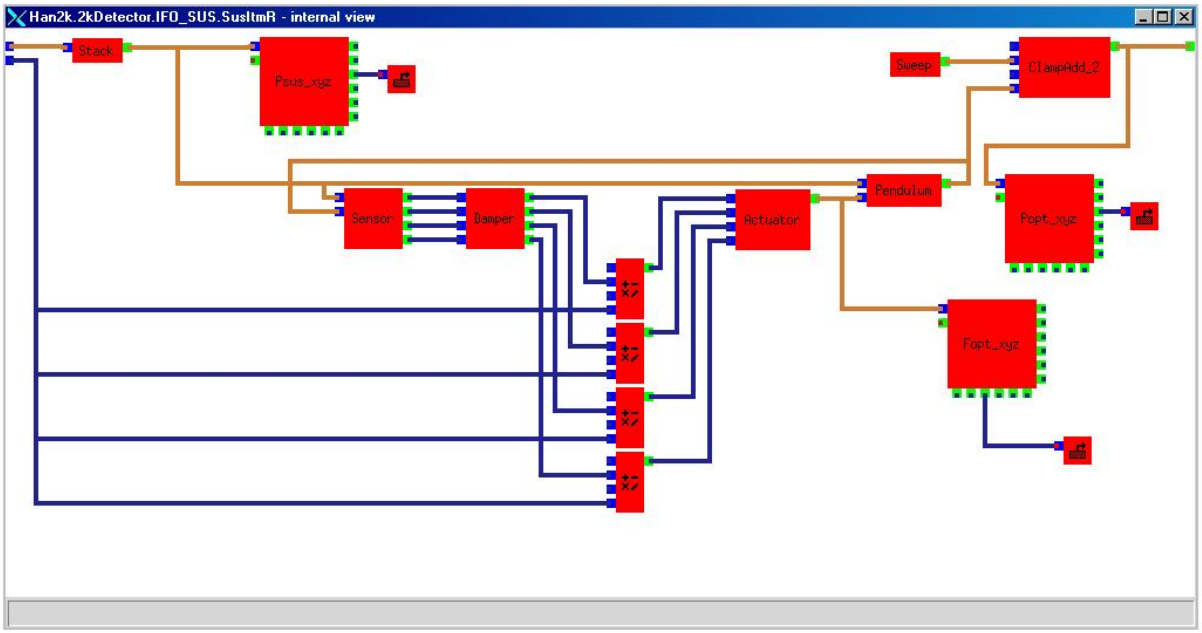

Figure 3.4: ITMR Suspension box.

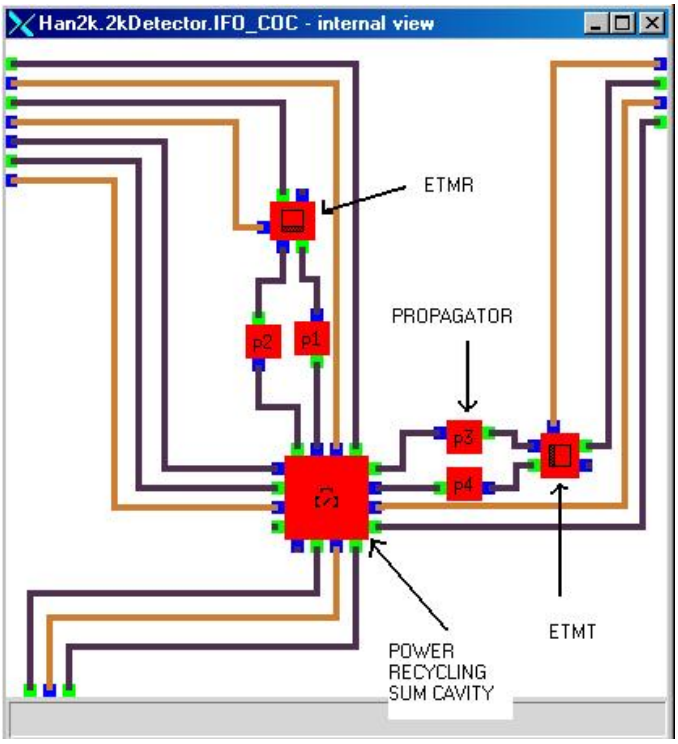

Figure 3.5: Core optical configuration.

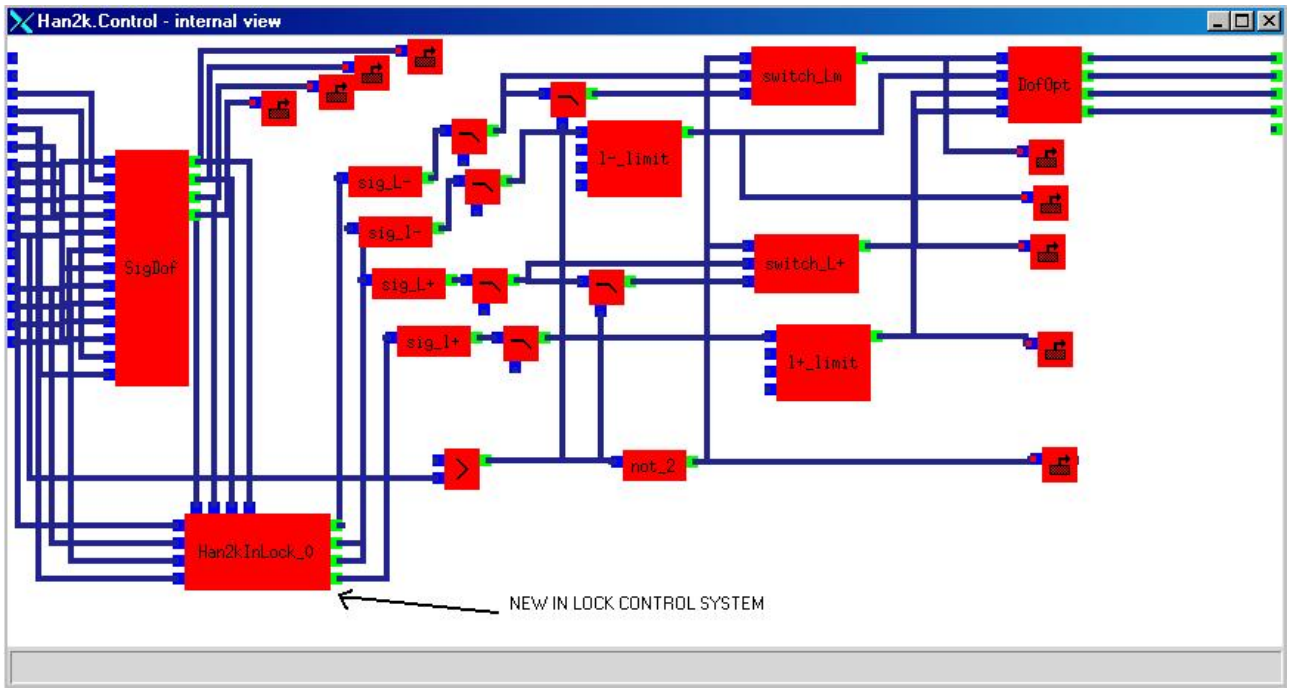

Figure 3.6: Control box.

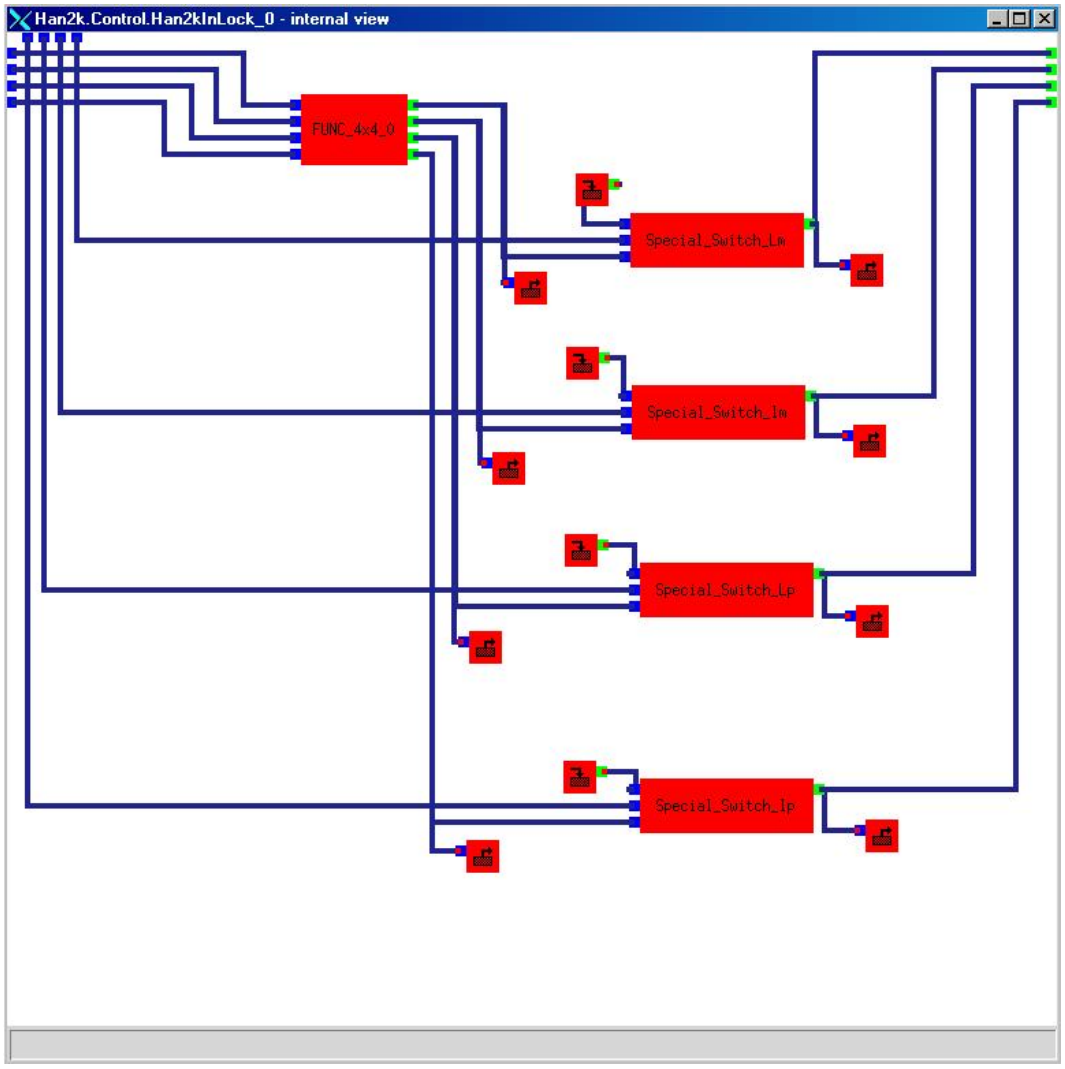

Figure 3.7: In Lock Control box.

This model is divided into two parts:

- the detector (2kdetector box (see figure 3.2)),
- the control system (Control box (see figure 3.6)).

The inputs are represented by blue pins and outputs by green pins.Blue wires represent the transfer of real values from one box to another and brown wires transfer of electric fields values. The model is built by wiring between the primitives defined by E2E. For each primitive, a set of parameters can be specified to match as much as possible to the reality. The dynamics of the system are represented by the field strengths in the propagators that can be seen in Figure 3.5.
the right par of figure 3.2 shows the optical sensors which look at all the output of the interferometer. The suspensions are composed of two parts: the first is the passive isolation from the floor through the stack and dampers (upper part of figure 3.4). the other shows how the control servo pushes against the pendulum to apply the corrections (lower part of 3.4). In the end, figure 3.6 shows how the control system has been designed. the upper left part of figure 3.6 contains the primitive which has been designed to acquiring lock. the lower left box is the control system we designed to keep lock. Then, the right part is a set of filters to adjust the control signals. As we will show later, this disposition of the “in lock” control matrix is not the best one because the filters are not really designed for this matrix. Figure 3.8 shows an attempt to design a complete control system with a control matrix (on the left), some filters (in the center) and another matrix to

convert the degrees of freedom to position of the mirrors. This version of the control box works only when the system is already in lock and we just try to keep lock. Remember what we want to do is to understand how to control Han2k in order to extend this analysis to dual recycling configuration.

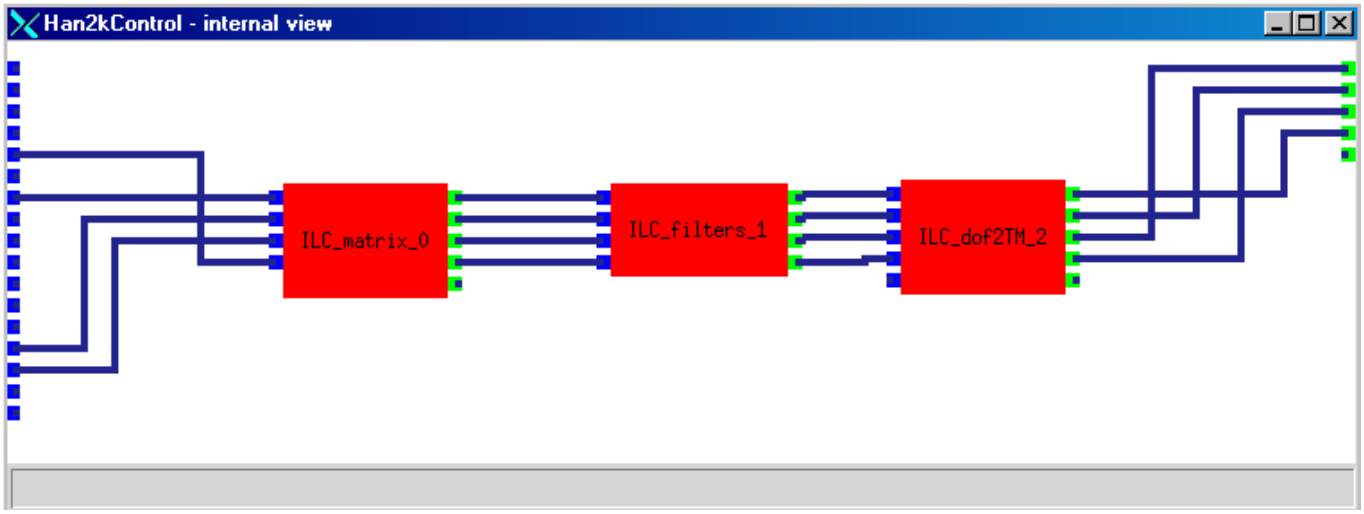

Figure 3.8: preliminary design of in lock control system for Han2k.

Figure 3.9 shows how the carrier and sideband fields grow in the various cavities and outputs from turn-on to full field strength as it is computed with E2E. The input power in 1W. The first graph shows the carrier field build up in the power recycling cavity. The sideband also build up but the input power for the sideband is much smaller than the carrier's. The sideband build up faster than the carrier because of the Pound-Drever lock acquisition method.This method is divided into 5 states in order to eliminate singularities of the control matrix:

- State 1: None of the degrees of freedom (DOFs) are controlled. This is the starting point for lock acquisition.
- State 2: The recycling cavity DOFs (l_- and l_+) are controlled and the sidebands are resonant in the power recycling cavity. The carrier is anti-resonant in this cavity. The control matrix is a 2×2 diagonal matrix.
- State 3: State 2 holds and one of the two arm cavity lengths is controlled. The carrier is resonant in the controlled arm cavity. the control matrix is divided into two matrix: one 1×1 for l_- and one 2×2 for l_+ and L_+.
- State 4: State 3 holds and the other arm cavity length is controlled. The carrier is resonant in the two arms so it flip the sign of the reflectivity of the compound mirror made by the two arms so the carrier is also resonant in the power recycling cavity. The control matrix is now 3×3 for l_+, L_+ and L_- and 1×1 for l_-. If the determinant of this 3×3 matrix goes too close to zero L_+ and l_+ cannot controlled in the same time. l_+ is left uncontrolled until the singularity passes.
- State 5: State 4 has endured long enough for the power level to equilibrate. This is the ending point for lock acquisition. The control matrix is a 4×4 matrix (No more singularity).

Figure 3.10 shows the different states of the lock acquisition path.
The sideband fields build up faster because they are anti-resonant in the arms so they just have to resonate in the power recycling cavity which is a short cavity. The carrier have to resonate first in the arms (long cavity) to be able to resonate in the power recycling cavity. The other graphs show the fields in other places in the interferometer.

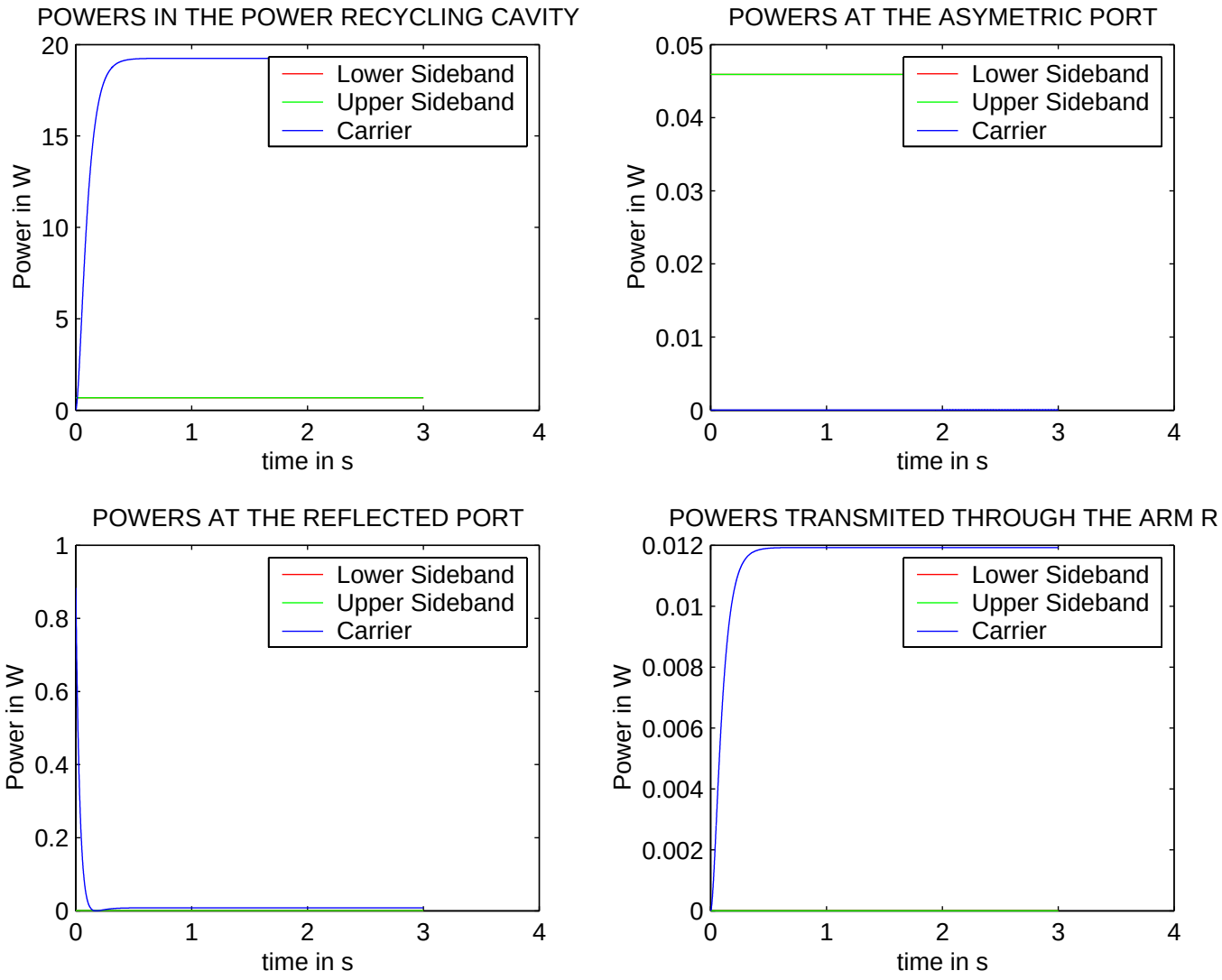

Figure 3.9: Powers in various cavities and outputs computed with E2E.

In this model, we use some approximations. The following list gives some of them:

- There is no angular misalignment during all the simulation.
- Scalar field approximation is used for electric field.
- The LASER is a regular LASER field generator and does not represent the Pre-Stabilized Laser (PSL) used in real Initial-LIGO and at the 40m prototype.
- The suspensions for the mirrors are simple pendula.
- The mirrors don't have any thickness.

Despite these limitations, E2E is a really useful tool to study LIGO-like interferometer and Matt Evans has proved it can be used to design the lock acquisition system [8]. Comparisons between E2E simulations and latest runs of real Initial-LIGO show that E2E can handle many aspects of the detectors and the fact that the Lock acquisition system designed with E2E is now used without any changes demonstrates its usefulness. Figure 3.10 shows how close E2E can be.

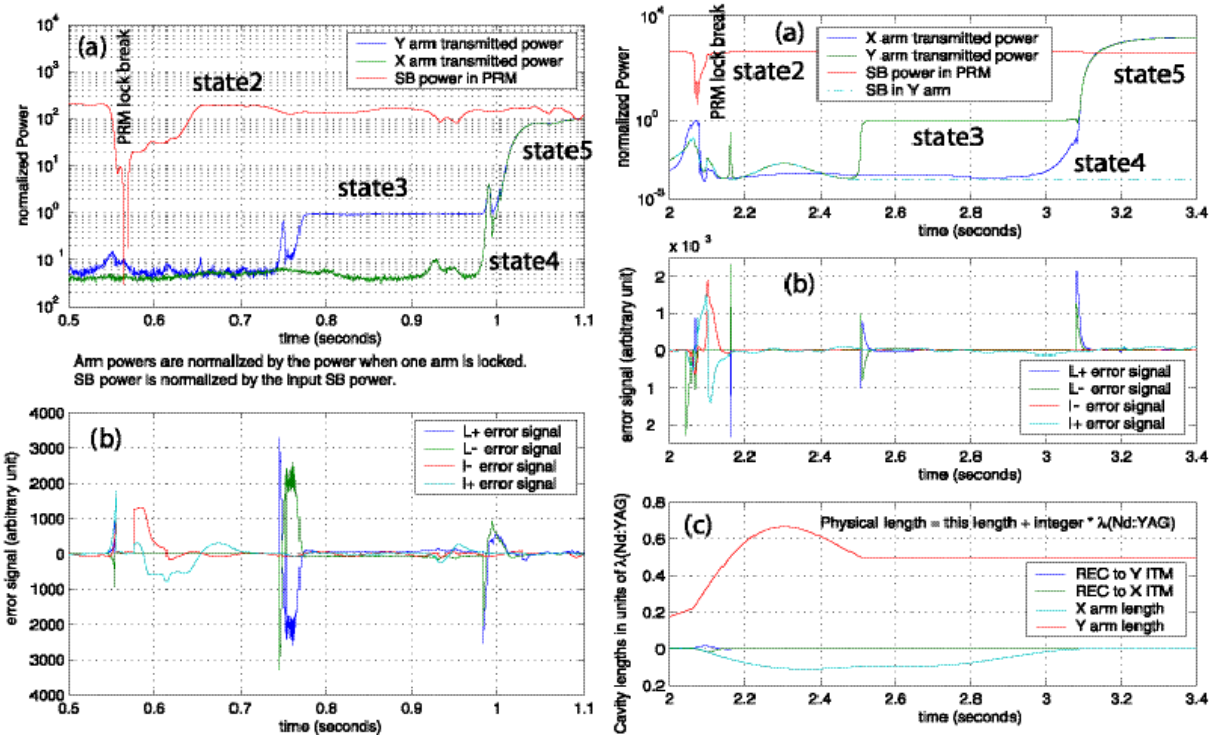

Figure 3.10: Comparison between E2E data and E2 real data [18].

Real antenna at the site are now in a phase of calibration and improvement of the sensitivity by fine tuning of the parameters of the detector. This phase will take about 6 months more and scientific runs will start in early 2002. E2E is a good tool to study how the interferometers are expected to perform in 6 months and new implementations in E2E will make it more realistic.

3.2 Theory of “in lock” control matrix:

The “in lock” control matrix is a matrix which can compute the corrections in the positions of the mirrors from the demodulated signals at the output of the interferometer in order to maintain lock. This matrix tells the control system how much to push against the pendulums the mirrors to compensate their motion due to noise or the presence of a gravitational wave. Ideally, the mirrors are always at the same position to keep the interferometer “in lock“ even if there is a gravitational wave passing through the detector. A measure of the noise and eventually of a gravitational wave is done in the error signals coming from the control matrix.
Initial-LIGO has four degrees of freedom we have to control:

- L_- differential mode of the arms,
- L_+ common mode mode of the arms,
- l_- differential mode of the Michelson interferometer,
- l_+ common mode of the Michelson interferometer.

L_-, L_+, and l_+ degrees of freedom are extensions of the standard Pound-Drever-Hall reflection locking technique. This means these degrees of freedom are controlled in a way to maintain the interferometer “in lock”. l_- Michelson degree of freedom is sensed via the "Schnupp transmission locking" scheme. This means l_- is controlled in a way to minimize the shift from the initial Schnupp asymmetry.
We measure S_j, the 6 demodulated signals at the output of the interferometer but for Initial-LIGO we use only 4:

- *AQ* signal at the anti-symmetric port quad-phase[1],
- *POBQ* signal at the pick off form the beam splitter in the direction of ITM_T quad-phase,
- *POBI* signal at the pick off form the beam splitter in the direction of ITM_T in-phase,
- *RI* signal at the symmetric port in-phase.

Each S_j can be decomposed in a sum of four signals S_{ij} coming from the excitation of each degrees of freedom. so S_{ij} is the signal at the demodulated signal j when only the degree of freedom i is excited and the others are null. We have:

$$S_j = \sum_{i=1}^{4} S_{ij} \tag{3.1}$$

we call G_{ij} the matrix obtained by taking the ratio of all the output signals S_{ij} by the input signals E_i (displacements of the mirror positions from their desired positions along the beam axis):

$$G_{ij} = \frac{S_{ij}}{E_i} \tag{3.2}$$

from eq. 3.1 and 3.2, we have:

$$S_j = \sum_{i=1}^{4} G_{ij} E_i \tag{3.3}$$

G is a constant matrix which does not depend of the inputs because the when the Michelson interferometer is “in lock” the system is linear. so if G has an inverse, we can compute the inputs signals E_i if we know G_{ij} by:

$$E = [G^{\top}]^{-1} S \tag{3.4}$$

To determine G, the best way is to move each degree of freedom at a time and measure the 6 output signals. With E2E, we can directly move the degrees of freedom with a sweep. G is obtained by taking the ratio of the output slope to the input slope. At the site we have to calibrate the detector: We must know how much current we need in the coil (actuator) to sweep exactly one fringe. we can deduce how much current we need to move the mirror by a known amount (which will be a function of frequency because we are pushing against a pendulum). After this extra step, we can drive each of the mirrors one at a time and see the effect at the output signals. we can easily pass from “moving one mirror” to “moving one degree of freedom” representation by a matrix which defines the degrees of freedom.

3.3 “In lock” control matrix measured with E2E:

E2E is a convenient way to measure the transfer function from any point of the detector to any other point. We used E2E to measure the transfer functions from each length degree of freedom to each output demodulated signal (in units of volts per meter), open loop and closed loop. We set the Han2k model to input a signal in a defined degree of freedom (e.g: $L\_$) with a sine wave form.

$$INPUT = A.sin(2\pi ft) \tag{3.5}$$

with $A = 10^{-11}$ and f which can vary from run to run. we run the simulation for 2 seconds and start to input a gravitational wave signal after one second in order to let the fields build up to their equilibrium values in all cavities (see figure 3.9). We assume the system is linear for at least a small perturbation so the output signal must be of the form:

$$OUTPUT = B_1(f).sin(2\pi ft) + B_2(f).cos(2\pi ft) \tag{3.6}$$

We use the expanded form in equation 3.6 because we can use linear method for regression. For each frequency f, we fit, using least square method, the output signal to the model in Eq.3.6 and extract the values of $B_1(f)$ and $B_2(f)$ for each frequencies. We can reconstruct the transfer function as

$$H(f) = \frac{B_1(f) + \imath B_2(f)}{A} \tag{3.7}$$

[1] In-phase and quad-phase mean the demodulation phase relative to the modulation placed on the input laser light by a phase-modulating pockels cell.

We obtained a 4×6 matrix of transfer functions open loop as table 3.1 shows. The X indicates transfer functions we could not fit to a simple model. transfer functions in the 2×2 upper left block in this table are understood as coming from the transfer function of the arms. The pole at $170Hz$ is exactly the cavity pole of the Fabry-Perot arms cavities. The others are not fully understood but the pole at $2.13Hz$ is the coupled cavity pole composed of the power recycling mirror and the rest of the interferometer.

DOF \ SIG	S_{AQ} (in V)	S_{AI} (in V)	S_{PQ} (in V)	S_{PI} (in V)	S_{SQ} (in V)	S_{SI} (in V)
L^- (in m)	$\frac{-1.5225e^{12}}{1+\imath\frac{f}{170\ Hz}}$	$\frac{8.1741e^{10}}{1+\imath\frac{f}{170\ Hz}}$	$\frac{-2.225e^{11}}{1+\imath\frac{f}{170\ Hz}}$	$\frac{-4.2013e^{12}}{1+\imath\frac{f}{170\ Hz}}$	X	X
l^- (in m)	$\frac{-3.0286e^{12}}{1+\imath\frac{f}{170\ Hz}}$	$\frac{1.6861e^{11}}{1+\imath\frac{f}{170\ Hz}}$	X	$\frac{-8.3696e^{12}}{1+\imath\frac{f}{170\ Hz}}$	$\frac{6.8920e^{9}(1+\imath\frac{f}{27\ Hz})}{1+\imath\frac{f}{2.13\ Hz}}$	X
L^+ (in m)	X	X	$\frac{-8.9090e^{12}}{1+\imath\frac{f}{2.13\ Hz}}$	$\frac{-1.6732e^{14}}{1+\imath\frac{f}{2.13\ Hz}}$	$\frac{4.0680e^{11}}{1+\imath\frac{f}{2.13\ Hz}}$	$\frac{-1.2541e^{12}}{1+\imath\frac{f}{2.13\ Hz}}$
l^+ (in m)	X	$\frac{5.1481e^{9}(1-\imath\frac{f}{370\ Hz})}{1+\imath\frac{f}{2.13\ Hz}}$	$\frac{-1.7768e^{13}(1+\imath\frac{f}{400\ Hz})}{1+\imath\frac{f}{2.13\ Hz}}$	$\frac{-3.3267e^{14}(1+\imath\frac{f}{770\ Hz})}{1+\imath\frac{f}{2.13\ Hz}}$	$\frac{8.0687e^{11}(1+\imath\frac{f}{2300\ Hz})}{1+\imath\frac{f}{2.13\ Hz}}$	$\frac{-2.4795e^{12}(1+\imath\frac{f}{950\ Hz})}{1+\imath\frac{f}{2.13\ Hz}}$

Table 3.1: fitted transfer function open loop with E2E.

We obtained the following bode plots of the complex transfer functions versus excitation frequency:

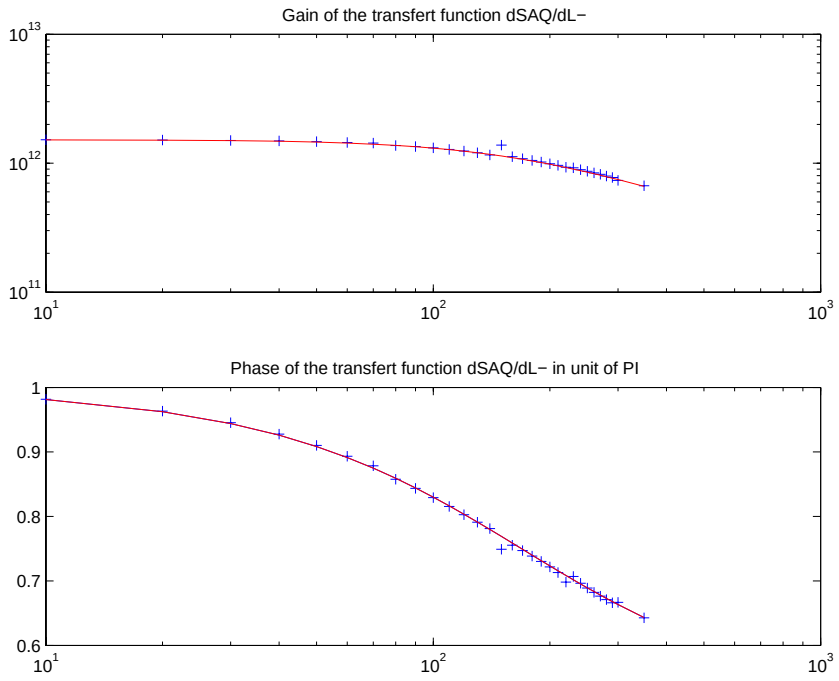

Figure 3.11: Transfer function open loop from L^- to S_{AQ}.

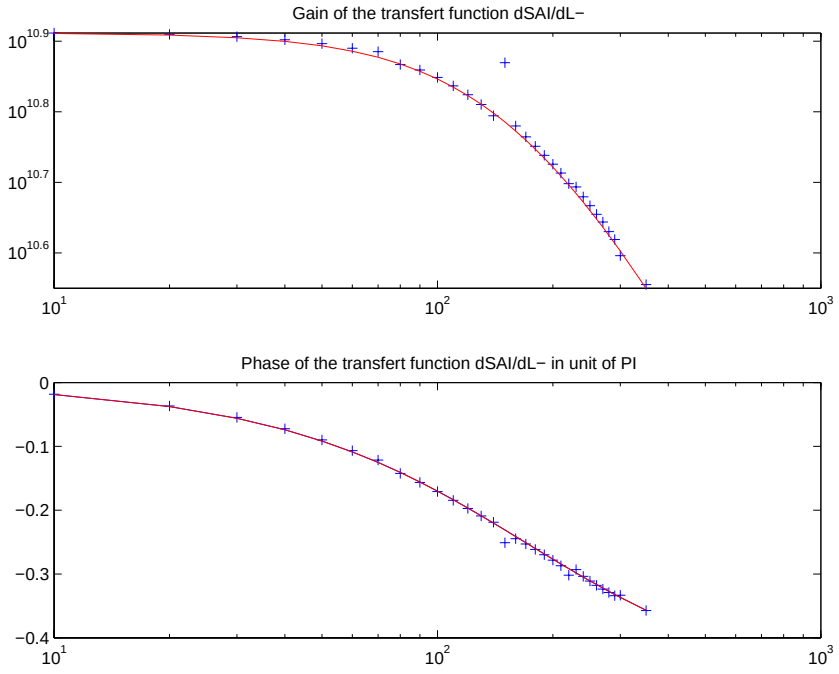

Figure 3.12: Transfer function open loop from L^- to S_{AI}.

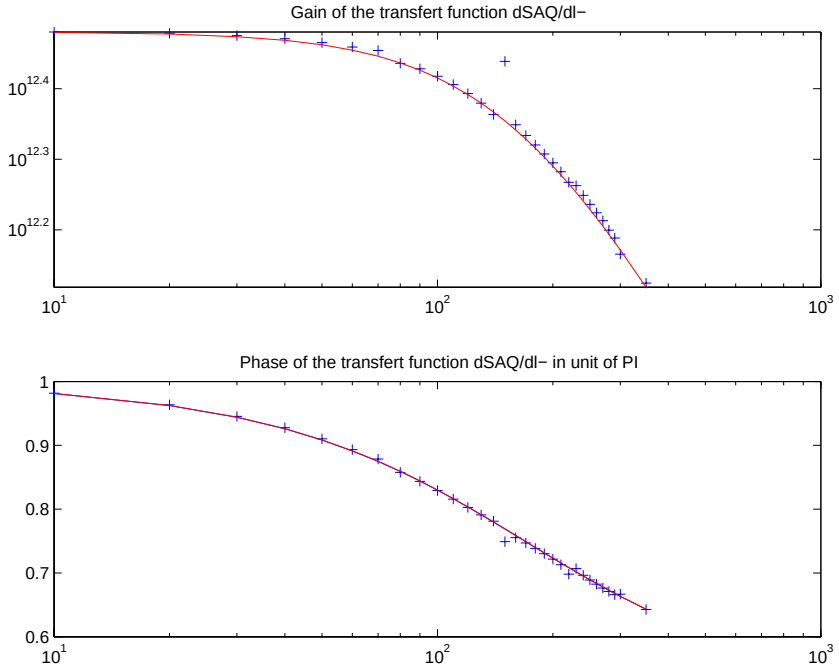

Figure 3.13: Transfer function open loop from l^- to S_{AQ}.

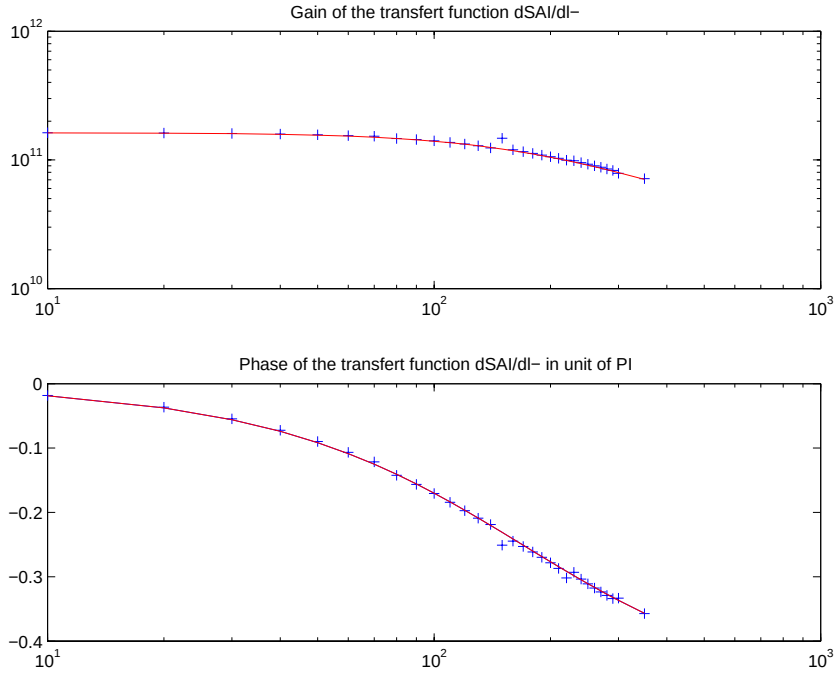

Figure 3.14: Transfer function open loop from l^- to S_{AI}.

The transfer functions measured closed-loop (ie, while the control system was activated) exhibit considerable complex structure, with many resonances, which are not yet fully understood.

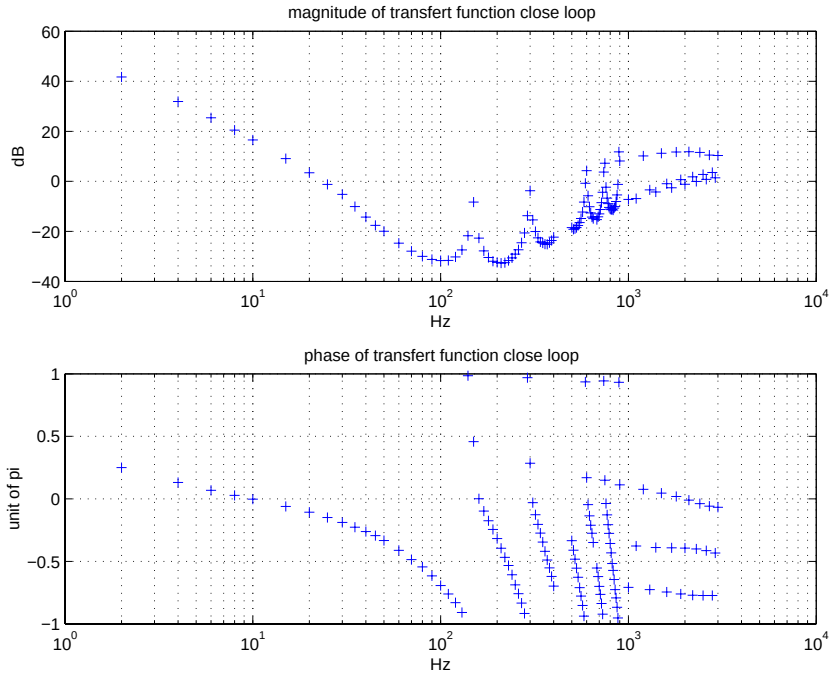

Figure 3.15: Transfer function close loop from L^- to S_{AQ}.

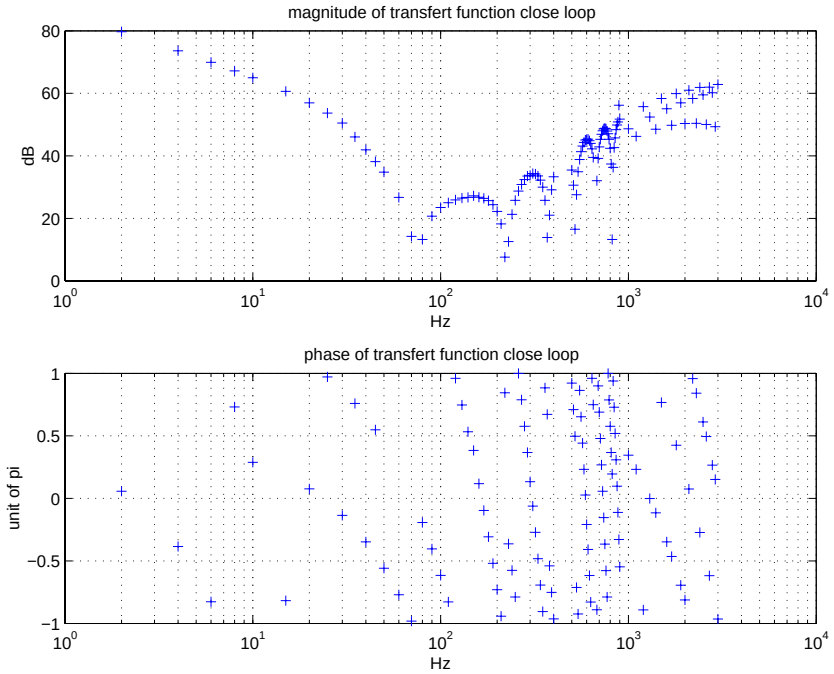

Figure 3.16: Transfer function close loop from L^- to S_{AI}.

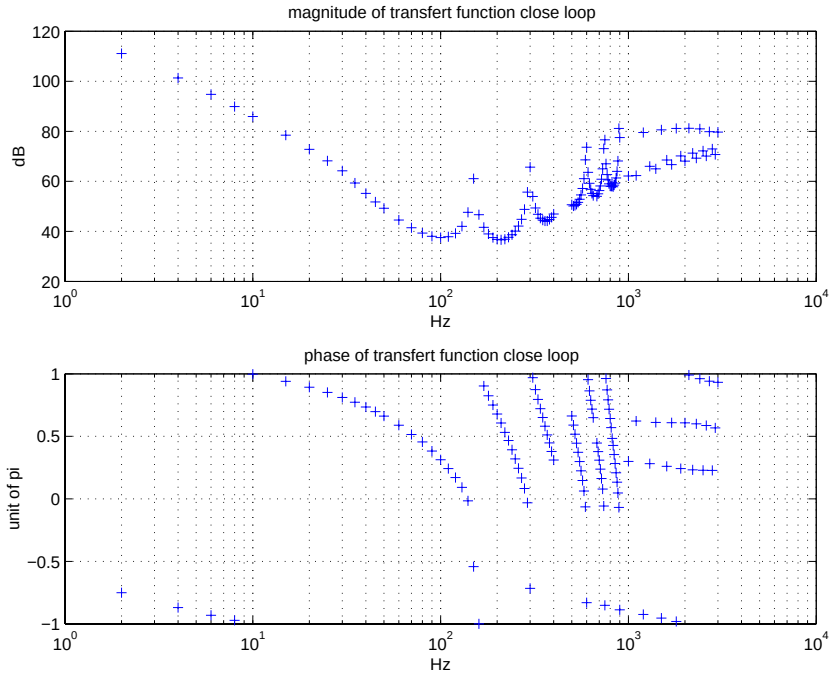

Figure 3.17: Transfer function close loop from L^- to S_{AQ}.

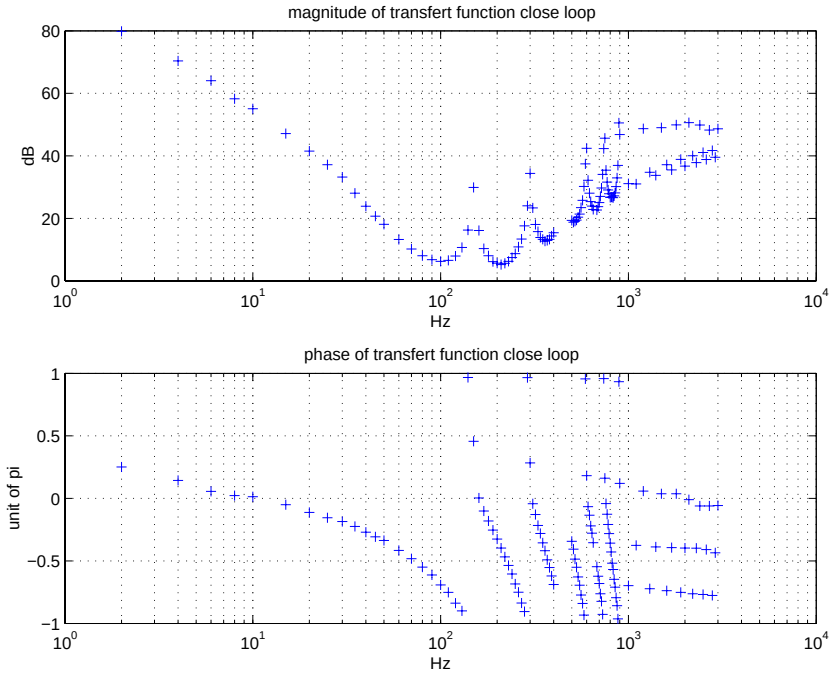

Figure 3.18: Transfer function close loop from L^- to S_{AI}.

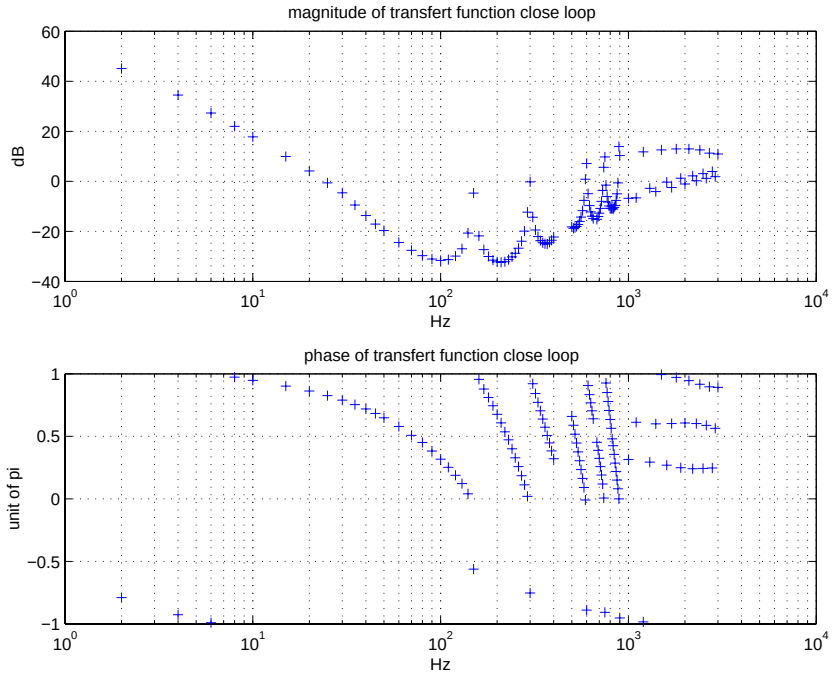

Figure 3.19: Transfer function close loop from L^- to S_{SQ}.

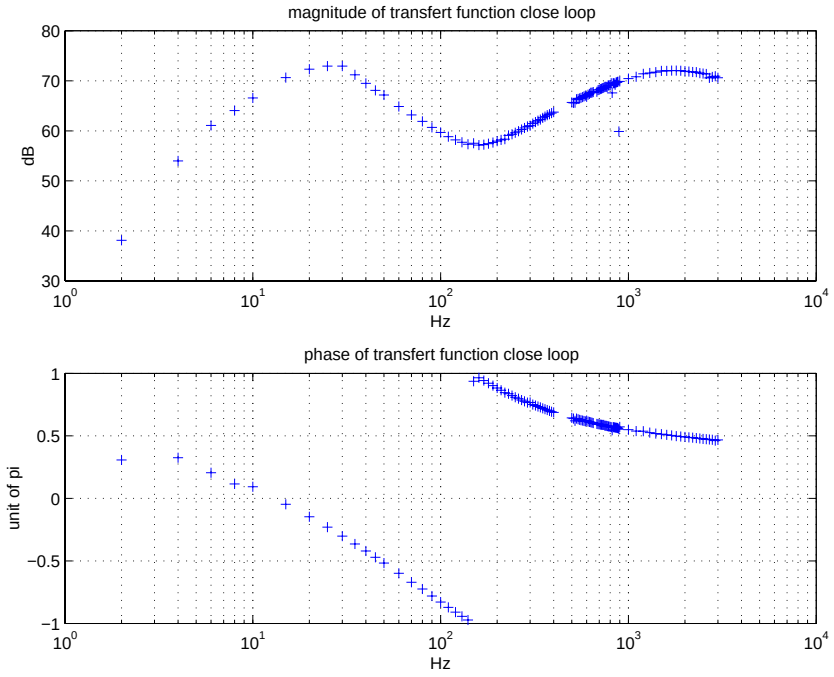

Figure 3.20: Transfer function close loop from L^- to S_{SI}.

Most of them show resonance at 150Hz and its harmonics but we do not yet understand where these come from. To measure the coefficient of the “in lock” control matrix we sweep each degree of freedom open loop slowly enough to remain “in lock” without the control system. We take the ratio of the blue slope with the red slope at 1s and this for each

combination of inputs and outputs. We obtained a 4×6 matrix and we extracted a 4×4 matrix G (AQ, POBQ, POBI and RI), inverted and transposed this matrix. The final matrix is the control matrix. Figure 3.21 shows the error signal for a sweep at the input:

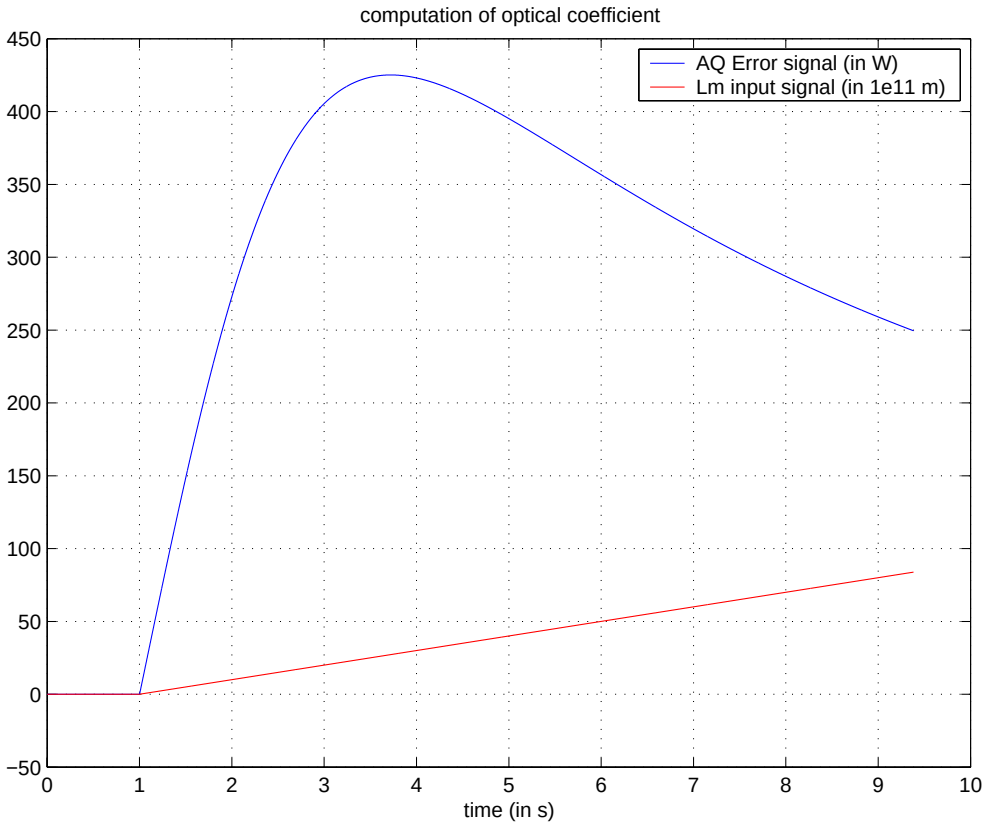

Figure 3.21: Error signal at the asymmetric port quad-phase for a sweep in L_{-}.

Table 3.2 shows this matrix:

0.00328358088609	−0.00002345359790	−0.00002620801951	0.00000019445135
−0.00020729195820	0.02909680679344	0.00000191128741	0.00029464475494
0.00000308836728	−0.00029815621959	−0.00002179992061	0.00179532349198
0.00061085707278	−0.08580272710334	0.00136174831372	0.23570672397610

Table 3.2: Control matrix (each coefficient must be multiplied by 10^{-10}).

This matrix is is roughly diagonal which is not a surprise because we extract the matrix G in choosing the signal where the degrees of freedom are the most “independent”.

3.4 Some results and problems

We tried to use this matrix to stay “in lock”. We compared the signals from the full control system system developed by Matt Evans [8] and the control matrix described here. Open loop and closed loop (with the full control system is use) the signals agree perfectly (at the precision of the machine) as figure 3.22 shows.

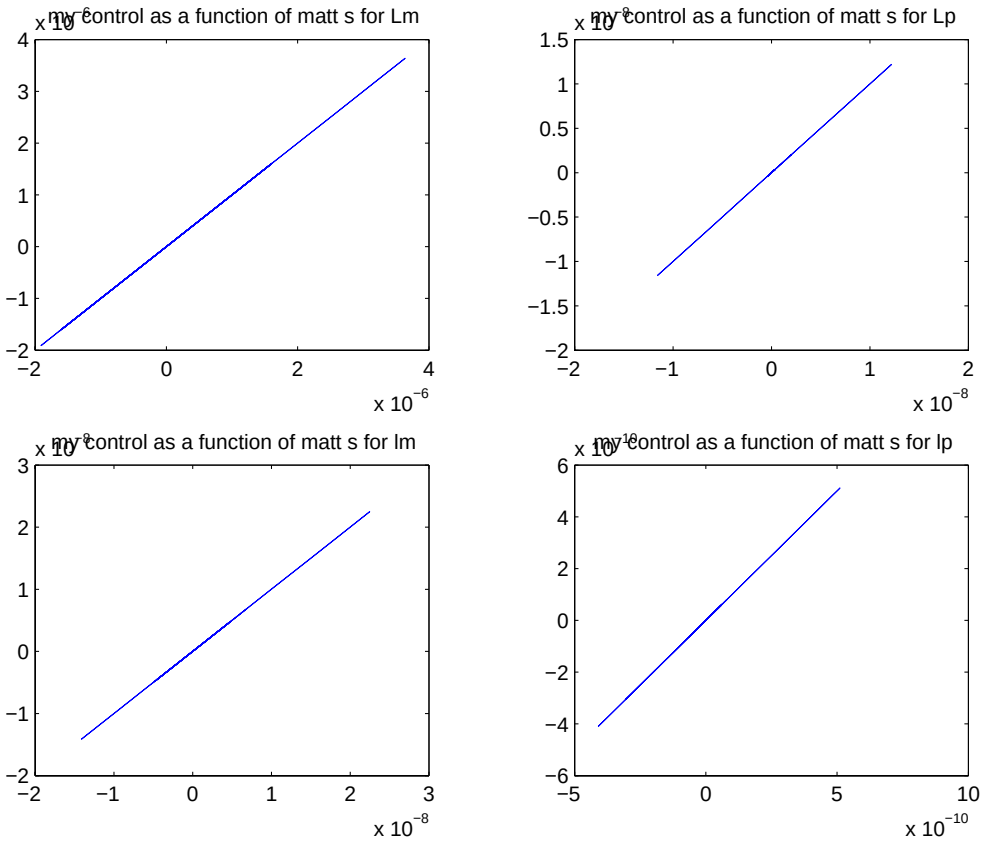

Figure 3.22: Comparison between full system and the new control system when the full control system is controlling.

But when we try to use our matrix to control, we do not control well and we loose some power in the power recycling cavity (shows that we loose lock see figure 3.23) and if the signal is to big (e.g: $L\_ = 10^{-9} sin(2\pi(20Hz)t)$) we loose lock completely.

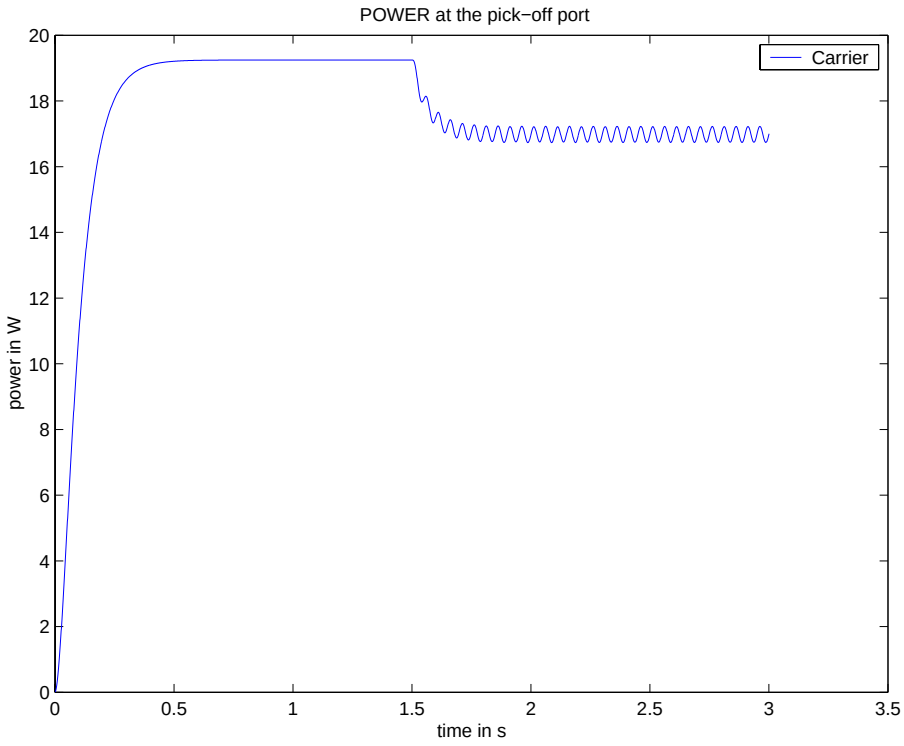

Figure 3.23: Power in the Power recycling cavity with a gravitational wave injected into L_- at 1.5s. Our control matrix cannot keep full lock but it is better than nothing.

The principal reason is the correction signals which reach the mirrors are too small (see figure 3.24):

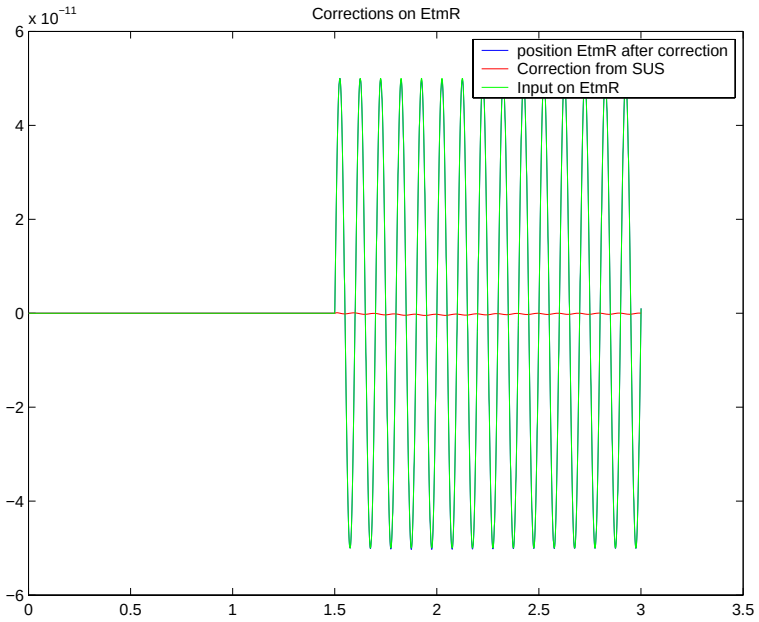

Figure 3.24: Correction directly applied to ETM_R.

Our last attempt to design a working control matrix could partially correct this effect. It seems the signals coming

from our control matrix are attenuated by the actuators and the pendulums in the suspensions. We tried to design the filters in the control system to compensate the effect of the actuators and the pendulums. We use the naive way, which is to set up the filters to have a transfer function inverse of the transfer function of the product of the actuator and the pendulum. we these filters our loop has too much gain and the control system kicks itself out of lock so we decreased the gain (multiplied by 0.53) and now the system is stable and can keep lock with an input $L\_ = 10^{-10} sin(2\pi(10Hz)t)\ m$ which was not possible before ; this is shown in figure 3.25.

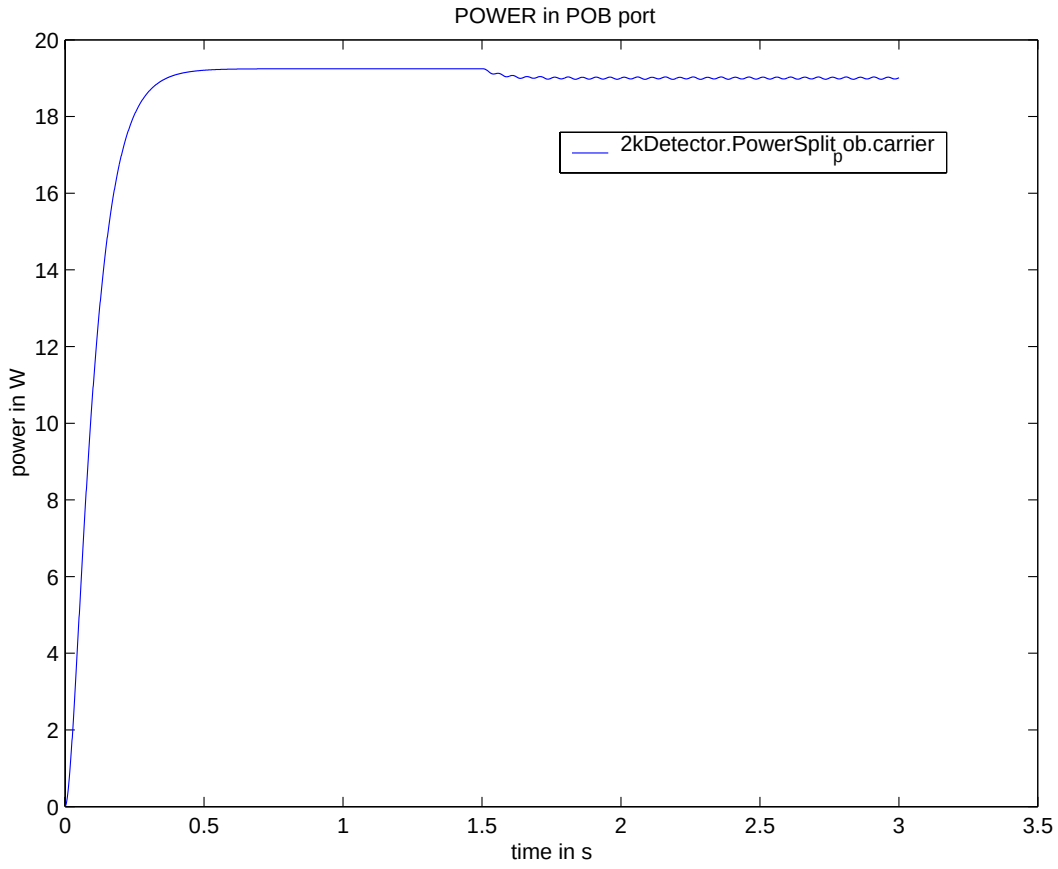

Figure 3.25: Power in the recycling cavity with a GW at 1.5s.

Figure 3.26 shows the real positions of the mirrors with an excitation of amplitude 10^{-10}. The motions of the mirrors have been attenuated by a factor 3.3 which is enough for the level of signal but not for bigger signals.

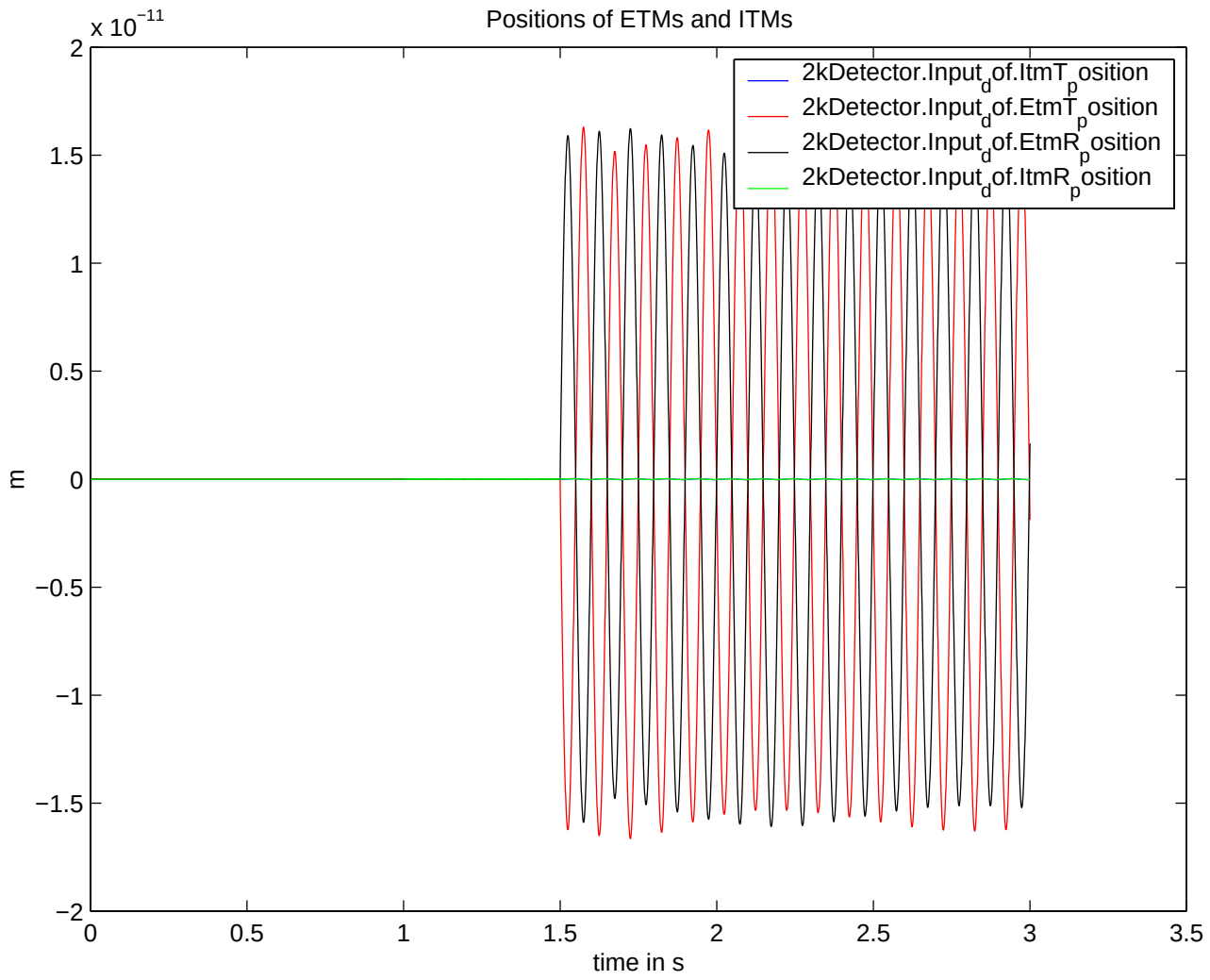

Figure 3.26: Positions of the mirrors with an excitation $L\_ = 10^{-10} sin(2\pi(10Hz)t)\ m$.

When looking how the correction is applied to the mirrors (e.g: ETM_R) we can see (see figure 3.27) that the correction is not perfect but the delay for the correction is extremely small (characteristic of system with light as way to measure).

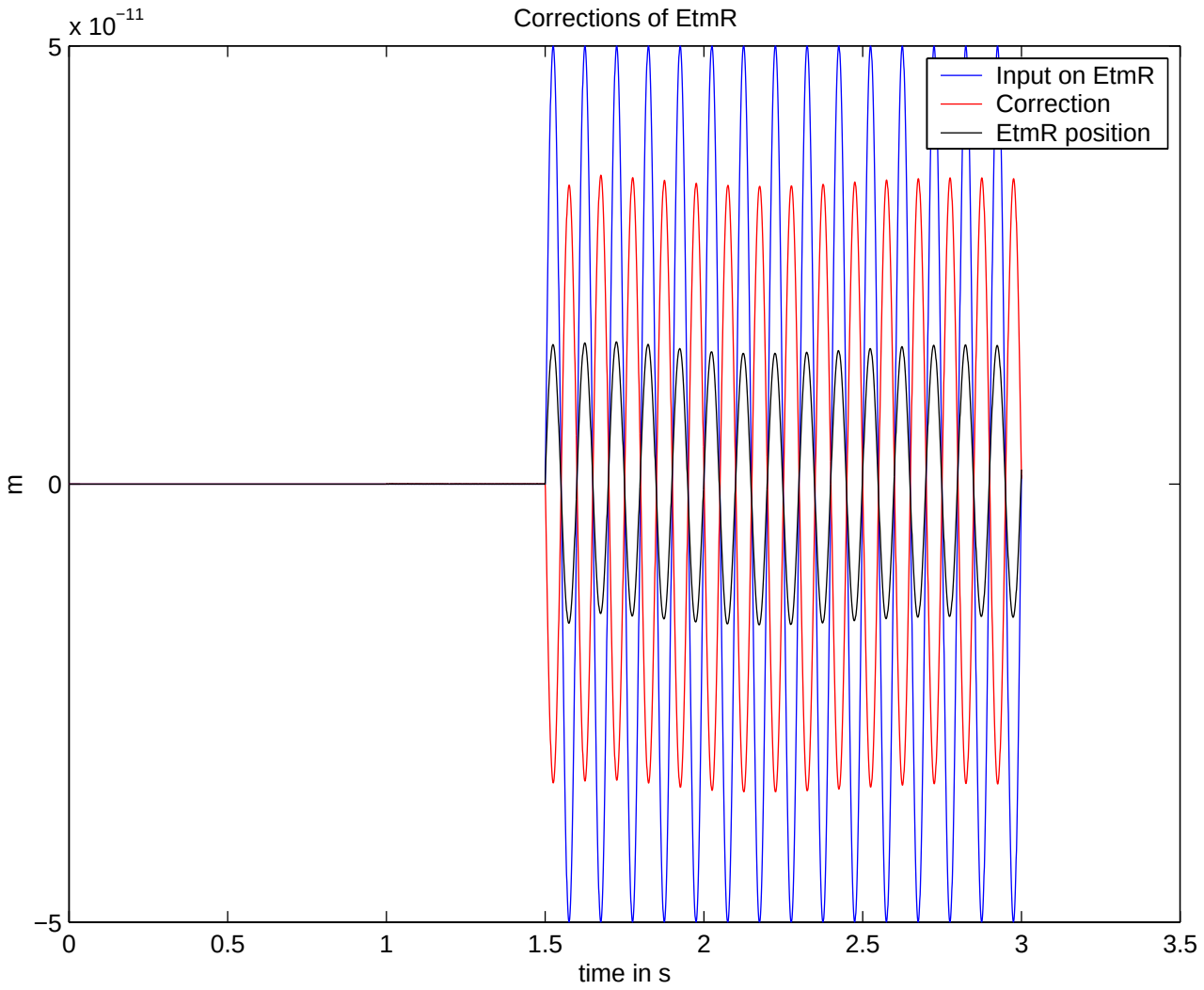

Figure 3.27: Correction on ETM_R with an input signal $L_- = 10^{-10} sin(2\pi(10Hz)t)\ m$.

Figures 3.25, 3.26 and 3.27 show we are on the road to find a way to design a control system to stay “in lock”. There remain problems: the system does not perform as well as the one designed by Matt Evans, and it is not yet clear why. Further, the problem of acquiring lock is not yet addressed by this control system.

Chapter 4

Conclusion

In this study, we have shown how to use the E2E simulation program with the Han2k model to simulate a LIGO-like interferometer.So far, we have simulated only the length degrees of freedom in order to develop a length sensing and control system. We have shown how to compute the “in lock” length control matrix to control the longitudinal motions of the core optics for Initial-LIGO. The latest simulations show that we can reduce by a factor of three the noise induced in the motion of the mirrors if we combine our control matrix and some frequency filters to compensate the pendula motion. This is not enough, but a deeper study of the filters should increase the efficiency of the length control system. I am confident because our control matrix seems to estimate with good precision the motion of the mirrors. The length control signal seems to degrade from the control matrix to the place where the corrections are applied (pendula). This fact is not fully understood and further work has to be done to understand and compensate for this effect.
This method can be generalized to Advanced-LIGO. It will just increase the size of the control matrix but there are no other fundamental difficulties. Further simulations have to be done to compute the “in lock” control matrix for Advanced-LIGO and we need to become more familiar with the DRLIGO model to implement the first length control system for Advanced-LIGO.
Personally, I learned a lot just by being in the laboratory and ask some questions about the interferometer. I shared my time between the simulations of the length control system and the life in the laboratory. The weekly meetings were a good opportunity to learn what was going on in the laboratory and discussions with Dennis UGOLINI (post-doc of the laboratory) and Steve VASS (manager of the laboratory) were a chance to deal with people who really construct the interferometer. The help of Alan WEINSTEIN has been precious to understand how LIGO works and what are the problems in an experimental laboratory.

Appendix A

Fabry-Perot cavity

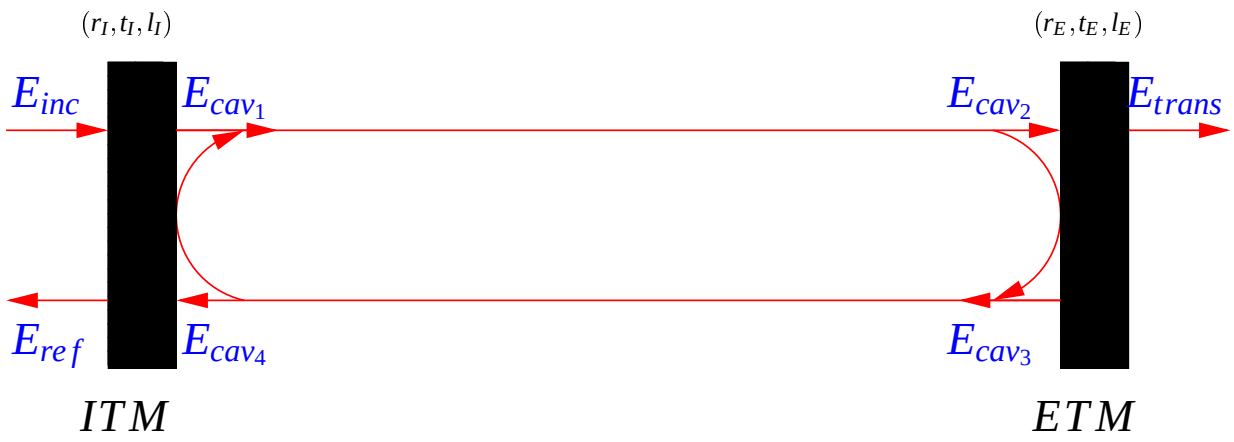

Figure A.1: Fabry-Perot cavity

The Fabry-Perot cavity is one of the principal building block of a gravitational wave interferometer. This appendix gives some results of the physics of Fabry-Perot cavity useful for the rest of the study.
We assume the efficiency of the photodetector equal to one. We neglect the thermal lensing effect of the mirrors due to the high power of the laser. We assume the input laser field is monochromatic. A generalization to non-monochromatic laser field is reached by summation of all components of the fields and in taking into account that the characteristics of the compound mirror is dependent on the frequency via k (wave number) of the input field.
We see a Fabry-Perot cavity can be reduced to one mirror with complex transmission t_{cav} and reflection r_{cav}.

A.1 Transmitted Field:

A fast calculation gives :

$$\frac{E_{trans}}{E_{inc}} = t_{cav} = \frac{t_E t_I e^{\imath\phi}}{1 - r_E r_I e^{2\imath\phi}} \tag{A.1}$$

A.2 Reflected Field:

A fast calculation gives:

$$\frac{E_{ref}}{E_{inc}} = r_{cav} = r_I - \frac{r_E t_I^2 e^{2\imath\phi}}{1 - r_E r_I e^{2\imath\phi}} \tag{A.2}$$

A.3 Properties:

- If $r_I, r_E \sim 1$ The field inside the cavity can be built up if $L = \frac{n}{2}\lambda$ where $n \in \mathbb{Z}$.

- If $r_I > (1 - l_I^2) r_E$, on resonance $r_{cav} > 0$ and the reflected field has the same sign as the input field. We say that the cavity is **undercoupled**.

- If $r_I < (1 - l_I^2) r_E$, on resonance $r_{cav} < 0$ and the reflected field has the opposite sign as the input field. We say that the cavity is **overcoupled**. This is how the LIGO arms are constructed.

A.4 Useful Parameters:

The **finesse** of a Fabry-Perot cavity is a parameter which shows how narrow the resonance of the cavity. The finesse F is a dimensionless parameter:

$$F = \frac{\pi\sqrt{r_I r_E}}{1 - r_I r_E}. \tag{A.3}$$

The finesse of the arms for LIGO is $F \sim 200$.

The **storage time** $\tau_{storage}$ of a Fabry-Perot cavity is the characteristic time for the cavity to empty if we turn off the input laser field:

$$\tau_{storage} = \frac{L}{c}\frac{F}{\pi} = \frac{L}{c}N\,, \tag{A.4}$$

where N is the **average number of bounces** in the cavity.

Because a Fabry-Perot cavity stores light, it stores energy. The **energy stored** in a Fabry-Perot cavity is proportional to the power going into the cavity, P_{inc}:

$$E_{stored} \propto \frac{|t_{cav}|^2}{|t_E|^2} P_{inc} \tau_{storage}. \tag{A.5}$$

Appendix B

Derivation of the gravitational wave equations

Einstein showed in 1915 his field equations [5]:

$$G_{\mu\nu} = 8\pi T_{\mu\nu}. \tag{B.1}$$

To derive gravitational wave's equations from eq.B.1, we use the linearized theory of gravity to the first order in $h_{\mu\nu}$ defined as:

$$g_{\mu\nu} = \eta_{\mu\nu} + h_{\mu\nu} \; with \; \mid h_{\mu\nu} \mid \ll 1, \tag{B.2}$$

where

$$\eta_{\mu\nu} = \begin{pmatrix} -1 & 0 & 0 & 0 \\ 0 & 1 & 0 & 0 \\ 0 & 0 & 1 & 0 \\ 0 & 0 & 0 & 1 \end{pmatrix} \tag{B.3}$$

is the metric in flat space-time. $g_{\mu\nu}$ is assumed to be symmetric for an isotropic universe so $h_{\mu\nu}$ is also symmetric.
For the solar system we have $\mid h_{\mu\nu} \mid \sim \mid \phi \mid \lesssim \frac{M_\odot}{R_\odot} \sim 10^{-6}$. So this theory is valid as long as we are in the solar system.

The general theory of Relativity gives us the way to calculate $G_{\mu\nu}$ through Ricci tensor $R_{\mu\nu}$:

$$G_{\mu\nu} = R_{\mu\nu} - \frac{1}{2} g_{\mu\nu} R \tag{B.4}$$

where $R = g^{\mu\nu} R_{\mu\nu} \sim \eta^{\mu\nu} R_{\mu\nu}$ to the first order in $h_{\mu\nu}$.

$$R_{\mu\nu} = \Gamma^{\alpha}{}_{\mu\nu,\alpha} - \Gamma^{\alpha}{}_{\mu\alpha,\nu} \tag{B.5}$$

where $\Gamma_{\mu\nu\rho}$ is the Christoffel symbol and $A_{\mu,\nu} = \partial_\nu A_\mu$.

$$\Gamma_{\mu\beta\gamma} = \frac{1}{2} g_{\mu\beta,\gamma} + g_{\mu\gamma,\beta} - g_{\beta\gamma,\mu} \tag{B.6}$$

So with eq B.2 and B.6 to first order in $h_{\mu\nu}$ we have :

$$\Gamma^{\gamma}{}_{\beta\gamma} = \frac{1}{2} \left(h^{\alpha}{}_{\beta,\gamma} + h^{\alpha}{}_{\gamma,\beta} - h_{\beta\gamma,}{}^{\alpha} \right), \tag{B.7}$$

$R_{\mu\nu}$ to first order in $h_{\mu\nu}$ is

$$R_{\mu\nu} = \frac{1}{2} \left(h^{\alpha}{}_{\nu,\mu\alpha} + h_{\mu\alpha,}{}^{\alpha}{}_{\nu} - h_{\mu\nu,}{}^{\alpha}{}_{\alpha} - h^{\alpha}{}_{\alpha,\mu\nu} \right), \tag{B.8}$$

and

$$R = h_{\alpha\gamma,}{}^{\alpha\gamma} - h_{,\alpha}{}^{\alpha}. \tag{B.9}$$

To simplify the result we introduce $\bar{h}_{\mu\nu}$ as :

$$\begin{cases} \bar{h}_{\mu\nu} = h_{\mu\nu} - \frac{1}{2} h \eta_{\mu\nu} \\ h_{\mu\nu} = \bar{h}_{\mu\nu} - \frac{1}{2} \bar{h} \eta_{\mu\nu} \end{cases} \tag{B.10}$$

Finally, to the first order in $h_{\mu\nu}$ Einstein's equation is

$$\frac{1}{2}\left(\bar{h}_{\alpha\nu,\mu}{}^{\alpha}+\bar{h}_{\alpha\mu,\nu}{}^{\alpha}-\bar{h}_{\mu\nu,\alpha}{}^{\alpha}-\eta_{\mu\nu}\bar{h}_{\alpha\gamma,}{}^{\alpha\gamma}\right)=8\pi T_{\mu\nu}. \tag{B.11}$$

This expression is gauge invariant. We can impose the gauge condition of Lorentz [1]:

$$\bar{h}_{\mu\alpha,}{}^{\alpha}=0 \tag{B.12}$$

and we obtain the field equations for gravitational wave in Lorentz's gauge:

$$\Box\bar{h}_{\mu\nu}=-16\pi T_{\mu\nu} \tag{B.13}$$

So we just have shown that Einstein's field equations can be reduce in linearized theory of gravity to wave equations with a source term represented by matter in the universe.

In vacuum Eq B.13 is reduced to :

$$\boxed{\Box\bar{h}_{\mu\nu}=0}. \tag{B.14}$$

We can find solutions as plane waves:

$$\bar{h}_{\mu\nu} = \mathrm{Re}\left(A_{\mu\nu}e^{\imath k_\alpha x^\alpha}\right), \tag{B.15}$$

$$k_\alpha k^\alpha = 0, \tag{B.16}$$

$$A_{\mu\nu}k^\nu = 0. \tag{B.17}$$

So the gravitational waves propagate with the speed of light and are transverse.

[1] this condition does not fix all the degrees of freedom due to the gauge symmetry and an additional condition can be chosen (see [5] for more details)

Bibliography

[1] Hiro YAMAMOTO Biplab BHAWAL, Malik RAHKMANOV and Matt EVANS. Physics of end-to-end model, 1997. LIGO internal note number T970196-00.

[2] Hiro YAMAMOTO Biplab BHAWAL, Malik RAHKMANOV and Matt EVANS. Alfi - the gui of end-to-end model, 1998. LIGO internal note number T980014-01.

[3] Hiro YAMAMOTO Biplab BHAWAL, Malik RAHKMANOV and Matt EVANS. Getting started with end-to-end model, 1998. LIGO internal note number T980051-00.

[4] Hiro YAMAMOTO Biplab BHAWAL, Malik RAHKMANOV and Matt EVANS. e2e primitive module - reference manual, 2000. LIGO internal note number T000047-01.

[5] Kip S. THORNE Charles W. MISNER and John A. WHEELER. *Gravitation.* Freeman, 1973.

[6] Benoit MOURS Michael LANDRY, Luca MATONE and Peter SHAWHAN. E2 amplitude calibration of the hanford recombined 2km ifo, 2001. LIGO internal note number G010057-00.

[7] Brett BOCHNER. *Modeling the Performance of Interferometric Gravitational-Wave Detectors with Realistically Imperfect Optics*. PhD thesis, California Institute of Technology, 1998. LIGO internal note number P980004-00.

[8] Matt EVANS. Automated control matrix system summary, April 2001. LIGO internal note number T000105-01.

[9] P. FRITSCHEL G. GONZALEZ A. MARIN N. MAVALAVALA D. OUIMETTE L. SIEVERS D. SIGG and M. ZUCKER. Length sensing and control subsystem preliminary design, 1997. LIGO internal note number T970122-00.

[10] Martin W. REGEHR. *Signal Extraction and Control for an Interferometric Gravitational Wave Detector*. PhD thesis, California Institute of Technology, 1994. LIGO internal note number P940002-00.

[11] Peter R. SAULSON. *Fundamentals of interferometric gravitational wave detectors*. World Scientific, 1994.

[12] Bernard F. SHUTZ and Massimo TINTO. Antenna patterns of interferometric detectors of gravitational waves. *Monthly Notices of the Royal Astronomical Society*, 224:131, 1987.

[13] K.A STRAIN. The ligo ii interferometer configuration, 1999. LIGO internal note number G990106-00.

[14] Kip THORNE. *Gravitational radiation.* Ellipse, 19??

[15] D. UGOLINI S. VASS A. WEINSTEIN M. SMITH J. ROMIE G. BILLINGSLEY and L. JONES. Conceptual design of the 40 meter laboratory upgrade for prototyping a advanced ligo interferometer, march 2001. LIGO internal note number T010029-DRAFT.

[16] Alan J. WEINSTEIN. Signal recycling cavity tune for 40m prototype of advanced ligo, April 2001. 40m lab internal note.

[17] Stan WHITCOMB. The ligo-i gravitational-wave detectors, February 2001. CaJAGWR Seminar - LIGO internal note number G010028-00.

[18] Hiro YAMAMOTO. Status of end to end model, 2001. LSC Meeting March 14 -17 2001 Livingston, LA - LIGO internal note number G010176-00.

[19] Hiro YAMAMOTO and Matt EVANS. Han2k - end user's guide, 2000. LIGO internal note number T000094-01.